

Towards Understanding Adversarial Transferability From Surrogate Training

Yechao Zhang^{*1 2 3 4}, Shengshan Hu^{*1 2 3 4}, Leo Yu Zhang[†], Junyu Shi^{*1 2 3 4}

Minghui Li[‡], Xiaogeng Liu^{*1 2 3 4}, Wei Wan^{*1 2 3 4}, and Hai Jin^{§1 2 5}

^{*} School of Cyber Science and Engineering, Huazhong University of Science and Technology

[†] School of Software Engineering, Huazhong University of Science and Technology

[‡] School of Information and Communication Technology, Griffith University

[§] School of Computer Science and Technology, Huazhong University of Science and Technology

{ycz, hushengshan, shijunyu220, minghuli, liuxiaogeng, weiwang_0303, hjin}@hust.edu.cn, leo.zhang@griffith.edu.au

Abstract—Adversarial examples for deep neural networks (DNNs) have been shown to be transferable: examples that successfully fool one white-box surrogate model can also deceive other black-box models with different architectures. Although a bunch of empirical studies have provided guidance on generating highly transferable adversarial examples, many of these findings fail to be well explained and even lead to confusing or inconsistent advice for practical use. In this paper, we take a further step towards understanding adversarial transferability, with a particular focus on surrogate aspects. Starting from the intriguing “little robustness” phenomenon, where models adversarially trained with mildly perturbed adversarial samples can serve as better surrogates to enhance transfer attack, we attribute it to a trade-off between two predominant factors: model smoothness and gradient similarity. Our investigations focus on their joint effects, rather than examining their separate correlations with transferability. Through a series of theoretical and empirical analyses, we conjecture that the data distribution shift induced by off-manifold samples in adversarial training is the key factor that impairs gradient similarity. Building on these two insights, we explore the impacts of prevalent data augmentation and gradient regularization methods on transferability and identify that this trade-off mechanism generally exists in the various training mechanisms, thus building a more comprehensive blueprint for the regulation mechanisms behind adversarial transferability. Finally, we provide a general route for constructing better surrogates to boost transferability which optimizes both model smoothness and gradient similarity simultaneously, e.g., the combination of input gradient regularization and sharpness-aware minimization (SAM), validated by extensive experiments. In summary, we call for attention to the united impacts of these two factors for launching effective transfer attacks, rather than optimizing one while ignoring the other, and emphasize the crucial role of manipulating surrogate models.

I. INTRODUCTION

Adversarial transferability is an intriguing property of adversarial examples (AEs), where examples crafted against a surrogate deep neural network (DNN) can fool other DNNs as well. Various techniques [12, 13, 22, 28, 40, 64, 70] have been proposed for the generation process of AEs to increase

transferability¹, such as integrating momentum to stabilize the update direction [12] or applying transformations at each iteration to create diverse input patterns [64]. At a high level, all these research endeavors to find transferable AEs under given surrogate models by proposing complex tricks to be incorporated into the generation pipeline one after another. However, this approach results in non-trivial computational expenses and low scalability [44].

With a different perspective, another line of work [] starts to examine the role of surrogate models. One useful observation is that attacking an ensemble of surrogate models with different architectures can obtain a more general update direction for AEs [5, 31]. A recent study [21] also proposed fine-tuning a well-trained surrogate to obtain a set of intermediate models that can be used for an ensemble. However, it remains unclear which type of surrogate performs the best and should be included in the ensemble. Our work taps into this line and tries to manipulate surrogates to launch stronger transfer attacks.

Meanwhile, Demontis *et al.* [9] started to explain the transferability property and showed that model complexity and gradient alignment negatively and positively correlate with transferability, respectively. Lately, Yang *et al.* [65] established a transferability lower bound and theoretically connect transferability to two key factors: model smoothness and gradient similarity. Model smoothness captures the general invariance of the gradient *w.r.t.* input features for a given model, while gradient similarity refers to the alignment of the gradient direction between surrogate and target models. However, there is still much to be understood and explored regarding these factors. For instance, it is unclear which factor plays a more important role in regulating transferability, how existing empirical findings for improving transferability affect these factors, and how to generally optimize them both simultaneously. Such a complex situation makes it challenging to completely understand the role of surrogates. Consequently, there is currently no consensus on how to construct better surrogates to achieve higher adversarial transferability. In support of this, a recent work [36], after performing a large-

¹National Engineering Research Center for Big Data Technology and System ²Services Computing Technology and System Lab ³Hubei Key Laboratory of Distributed System Security ⁴Hubei Engineering Research Center on Big Data Security ⁵Cluster and Grid Computing Lab

¹We refer to “adversarial transferability” as “transferability” in this paper.

TABLE I: The overview of our interactions with literature in the field.

Existing conclusions and viewpoints	Our observations and inferences	Relation
Stronger regularized (smoother) models provide better surrogates on average [9].	(1) <i>AT</i> with large budget yields smoother models that degrade transferability. In Sec. II-A. (2) Stronger regularizations cannot always outperform less smooth solutions like <i>SAM</i> . In Sec. IV-C.	Partially conflicting
<i>AT</i> and data augmentation do not show strong correlations to transfer attacks in the “real-world” environment [36].	(1) <i>AT</i> with small budget benefits transfer attack while large budget hinders it. (2) Data augmentation generally impairs transfer attacks, especially for stronger augmentations. In Sec. VI, Q6.	Conflicting
Surrogate models with better generalization behavior could result in more transferable AEs [58].	Data augmentations that yield surrogates with the best generalization perform the worst in transfer attacks. In Sec. VI, Q4.	Conflicting
Attacking multiple surrogates from a sufficiently large geometry vicinity (LGV) benefits transferability [21].	Attacking multiple surrogates from arbitrary LGV of a single superior surrogate may degrade transferability. In Sec. V-B.	Partially conflicting
Regularizing pressure transfers from the weight space to the input space. [11].	This transfer effect exists, yet is marginal and unstable. In Sec. IV-B.	Partially conflicting
The poor transferability of ViT is because existing attacks are not strong enough to fully exploit its potential [41].	The transferability of ViT may have been restrained by its default training paradigm. In Sec. VI, Q5	Parallel
Model complexity (the number of local optima in loss surface) correlates with transferability [9].	A smoother model is expected to have less and wider local optima in a finite space. In Sec. VI, Q3	Causal
AEs lie off the underlying manifold of clean data [20].	Adversarial training causes data distribution shift induced by off-manifold AEs, thus impairing gradient similarity.	Dependent
(1) Attacking an ensemble of surrogates in the distribution found by <i>Bayes</i> learning improves the transferability [29]. (2) <i>SAM</i> can be seen as a relaxation of <i>Bayes</i> [39].	<i>SAM</i> yields general input gradient alignment towards every training solution. Attacking <i>SAM</i> solution significantly improves transferability. In Sec. VI, Q7.	Matching

scale empirical study in real-world settings, concluded that surrogate-level factors that affect the transferability highly chaotically interact and there is no effective solution to obtain a good surrogate except through trial and error.

In light of this, we aim to deepen our understanding of adversarial transferability and provide concrete guidelines for training better surrogates for improving transferability. Specifically, we offer the following contributions:

Gaining a deeper understanding of the “little robustness” phenomenon. We begin by exploring the intriguing “little robustness” phenomenon [51], where models produced by small-budget adversarial training (*AT*) serve as better surrogates than normally trained ones (see Fig. 2). Through tailored definitions of gradient similarity and model smoothness, we recognize this phenomenon comes along with an inherent trade-off effect between these two factors on transferability. Thus we attribute the “little robustness” appearance to the persistent improvement of model smoothness and deterioration of gradient similarity. Further, we identify the observed gradient dissimilarity in *AT* as the result of the data distribution shift caused by off-manifold samples.

Investigating the impact of data augmentation on transferability. Beyond *AT*, we explore more general distribution shift cases to confirm our hypothesis on data distribution shift impairing gradient similarity. Specifically, we exploit four popular data augmentation methods, Mixup (*MU*), Cutmix (*CM*), Cutout (*CO*), and Label smoothing (*LS*) to investigate how these different kinds of distribution shifts affect the gradient similarity. Extensive experiments reveal they unanimously impair gradient similarity in different levels, and the degradation generally aligns with the augmentation magnitude. Moreover, we find different augmentations affect smoothness

differently. While *LS* benefits both datasets, other methods mostly downgrade smoothness in CIFAR-10 and show chaotic performance in ImageNette. Despite their different complex trade-off effects of similarity and smoothness, they generally yield consistent degradations in transferability.

Investigating the impact of gradient regularization on transferability. As the concept of gradient similarity is inherently tangled up with unknown target models, it is difficult to directly optimize it in the real scenario. Therefore, we explore solutions that presumably feature better smoothness without explicitly changing the data distribution, *i.e.*, gradient regularization. Concretely, we explore the impact of four gradient regularizations on model smoothness: input gradient regularization (*IR*) and input Jacobian regularization (*JR*) in the input space, and explicit gradient regularization (*ER*) and sharpness-aware minimization (*SAM*) in the weight space. Our extensive experiments show that gradient regularizations universally improve model smoothness, with regularizations in the input space leading to faster and more stable improvement than regularizations in the weight space. However, while input space regularizations (*JR*, *IR*) produce better smoothness, they do not necessarily outperform weight space regularizations like *SAM* in terms of transferability. We also find this aligns with the fact that they weigh differently on gradient similarity, which plays another crucial role in the overall trade-off.

Proposing a general route for generating surrogates. Considering the practical black-box scenario, we propose a general route for the adversary to obtain surrogates with both superior smoothness and similarity. This involves first assessing the smoothness of different training mechanisms and comparing their similarities, then developing generally effective strategies by combining the best elements of each.

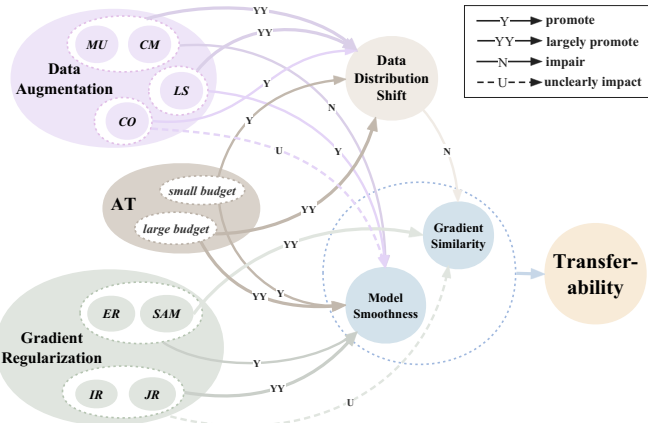


Figure 1: A complete overview of the relationship between factors regulating adversarial transferability of our study.

Our experimental results show that input regularization and *SAM* excel at promoting smoothness and similarity, respectively, as well as other complementary properties. Thus, we propose *SAM&JR* and *SAM&IR* to obtain better surrogates. Extensive results show our methods significantly outperform existing solutions in boosting transferability. Moreover, we showcase that the design is a plug-and-play method that can be directly integrated with surrogate-independent methods to further improve transferability. The transfer attack results on three commercial Machine-Learning-as-a-Service (MLaaS) platforms also demonstrate the effectiveness of our method against real-world deployed DNNs.

In summary, we study the complex trade-off between model smoothness and gradient similarity (see Fig. 1) under various circumstances and identify a general alignment between the trade-off and transferability. We call for attention that, for effective surrogates, one should handle these two factors well. Throughout our study, we also discover a range of observations correlating existing conclusions and viewpoints in the field, Tab. I provides a glance at them and report the relations.

II. EXPLAINING LITTLE ROBUSTNESS

Understanding adversarial transferability is still a challenging task, and many empirical observations in the literature are rather perplexing. As a typical case, “*little robustness*” indicates that a model adversarially trained with small perturbation budgets improves the transferability [51, 52]. It remains unclear why small-budget adversarially trained models can serve as better surrogates, whereas large-budget ones do not exhibit this benefit (see Fig. 2). In this section, we tailor the definitions of gradient similarity and model smoothness, two recently proposed concepts that are believed to be important for transferability [65], to analyze this phenomenon.

Notations. We denote the input space as $\mathcal{X} = \mathbb{R}^d$, and the output space as $\mathcal{Y} = \mathbb{R}^m$. We also consider a standard classification training dataset $\mathbf{S} = \{(x_1, y_1), \dots, (x_n, y_n)\}$, where $x_i \in \mathcal{M} \subset \mathcal{X}$ and $y_i \in \mathcal{L} = \{(0, 1)^m\} \subset \mathcal{Y}$ are *identically and independently distributed* (i.i.d.) drawn from the normal

data distribution $\mathcal{D} \in \mathcal{P}_{\mathcal{X} \times \mathcal{Y}}$. \mathcal{M} denotes the normal (image) feature manifold, \mathcal{D} is supported on $(\mathcal{M}, \mathcal{L})$ and $\mathcal{P}_{\mathcal{X} \times \mathcal{Y}}$ is the set of distributions on $\mathcal{X} \times \mathcal{Y}$. We further denote the marginal distribution on \mathcal{X} and \mathcal{Y} as $\mathcal{P}_{\mathcal{X}}$ and $\mathcal{P}_{\mathcal{Y}}$, respectively. The classification model can be viewed as a mapping function $\mathcal{F} : \mathcal{X} \rightarrow \mathcal{L}$. Specifically, given any input $x \in \mathcal{X}$, \mathcal{F} will find an optimal match $\mathcal{F}(x) = \arg \min_{y \in \mathcal{L}} \ell_{\mathcal{F}}(x, y)$ with the hard labels \mathcal{L} , where $\ell_{\mathcal{F}} : \mathcal{X} \times \mathcal{Y} \rightarrow \mathbb{R}_+$ can be decomposed to a training loss ℓ^2 and the network’s logits output $f(\cdot)$: $\ell_{\mathcal{F}}(x, y) := \ell(f(x), y)$, $(x, y) \in (\mathcal{X}, \mathcal{Y})$.

In this paper, we denote the surrogate model and target model as \mathcal{F} and \mathcal{G} , respectively. Generally, both \mathcal{F} and \mathcal{G} can be trained within the data distribution \mathcal{D} using \mathbf{S} , or a close yet different distribution \mathcal{D}' obtained by a specific augmentation mechanism on \mathbf{S} . Throughout this paper, we use \mathcal{D}' to denote a data distribution different from \mathcal{D} . Since this paper focuses on studying the transferability from the surrogate perspective, we assume \mathcal{G} is also well-trained on \mathcal{D} by default. We defer the analysis and experimental results when \mathcal{G} is trained on various \mathcal{D}' to Sec. VI, Q2, where the results also support the conclusions drawn from the case of \mathcal{D} .

A. Adversarial Transferability of Adversarial Training

Adversarial training [34] (AT) uses adversarial examples generated on \mathbf{S} as augmented data and minimizes the following adversarial loss:

$$L_{adv} = \frac{1}{\|\mathbf{S}\|} \sum_{i=1}^{\|\mathbf{S}\|} \max_{\|\delta\|_2 \leq \epsilon} \ell(f(x_i + \delta), y_i), \quad (1)$$

where $\delta \in \mathbb{R}^d$ denotes the adversarial perturbation and ϵ is the adversarial budget. As evidenced by our experiments in Fig. 2, the attack success rates (ASRs) arise with relatively small-budget adversarially trained models and start to decrease with the high-budget ones. This “transferability circuit” is particularly intriguing. We thus revisit the recently proposed transferability lower bound [65] and utilize it as a tool to analyze the underlying reason.

B. Lower Bound of Transferability

We first re-define model smoothness and gradient similarity, as well as the transferability between two models, based on which a lower bound of transferability could be obtained.

Definition 1 (Model smoothness). Given a model \mathcal{F} and a data distribution \mathcal{D} , the model smoothness of \mathcal{F} on \mathcal{D} is defined as $\sigma_{\mathcal{F}, \mathcal{D}} = \mathbb{E}_{(x, y) \sim \mathcal{D}} [\sigma(\nabla_x^2 \ell_{\mathcal{F}}(x, y))]$, where $\sigma(\cdot)$ denotes the **dominant eigenvalue**, and $\nabla_x^2 \ell_{\mathcal{F}}(x, y)$ is the Hessian matrix w.r.t. x . We abbreviate $\sigma_{\mathcal{F}, \mathcal{D}}$ as $\sigma_{\mathcal{F}}$ for simplicity and further define the upper smoothness as $\bar{\sigma}_{\mathcal{F}} = \sup_{(x, y) \sim \mathcal{D}} \sigma(\nabla_x^2 \ell_{\mathcal{F}}(x, y))$, where \sup is the supremum function.

Model smoothness refers to the ability of a model to produce a smooth loss surface on average across the input space. A smoother model on \mathcal{D} is featured with smaller $\sigma_{\mathcal{F}}$ and $\bar{\sigma}_{\mathcal{F}}$,

²We use the cross-entropy loss by default in the paper.

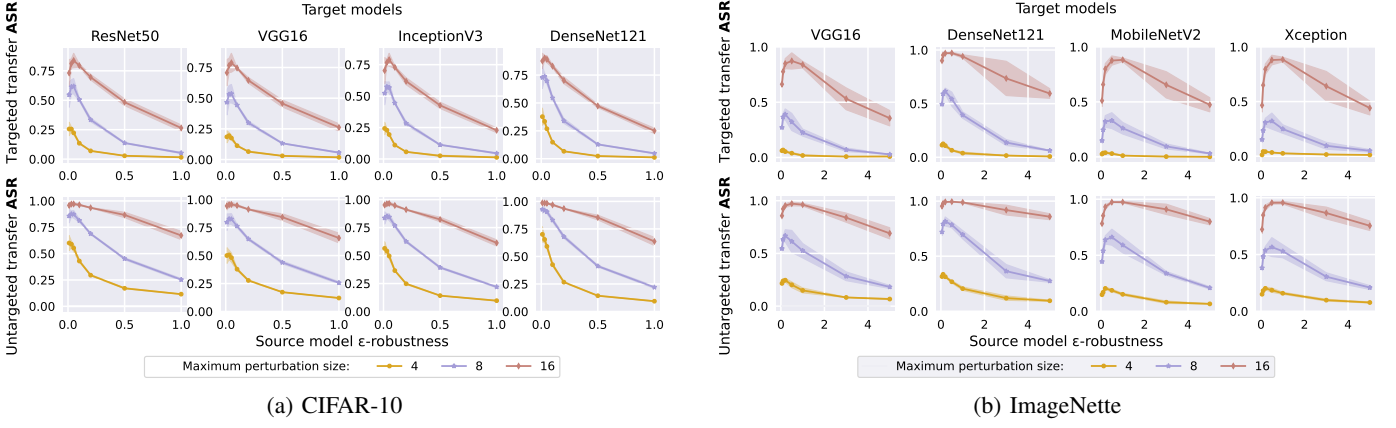


Figure 2: Transfer attack success rates (ASRs) against adversarially trained CIFAR-10 and ImageNette classifiers. We plot the average results of different surrogates obtained by 3 random seeds and the corresponding error bars for each ϵ .

indicating more invariance of loss gradient. Different from its original definition where the global Lipschitz constant $\beta_{\mathcal{F}}$ is used [65], we use this curvature metric (*i.e.*, the dominant eigenvalue of the Hessian) to define the model smoothness in a local manner. With this modified definition, we can theoretically and empirically quantify the smoothness of loss surface on \mathcal{F} for a given data distribution \mathcal{D} . Moreover, this provides a tighter bound for the model’s loss function gradient, namely, an explicit relation $\bar{\sigma}_{\mathcal{F}} \leq \beta_{\mathcal{F}}$ holds. Although the true distribution \mathcal{D} is unknown, one can still sample a set of data from \mathcal{S} and use the empirical mean as an approximation to evaluate the model smoothness. Note that our definition is correlated to the model complexity concept introduced in Demontis *et al.* [9] (see Sec. VI, Q3).

Definition 2 (Gradient similarity). For two models \mathcal{F} and \mathcal{G} with the loss functions $\ell_{\mathcal{F}}$ and $\ell_{\mathcal{G}}$, the gradient similarity over (x, y) is defined as $\mathcal{S}(\ell_{\mathcal{F}}, \ell_{\mathcal{G}}, x, y) = \frac{\nabla_x \ell_{\mathcal{F}}(x, y) \cdot \nabla_x \ell_{\mathcal{G}}(x, y)}{\|\nabla_x \ell_{\mathcal{F}}(x, y)\|_2 \|\nabla_x \ell_{\mathcal{G}}(x, y)\|_2}$.

Given a distribution \mathcal{D} , we can further define the infimum of loss gradient similarity on \mathcal{D} as $\underline{\mathcal{S}}_{\mathcal{D}}(\ell_{\mathcal{F}}, \ell_{\mathcal{G}}) = \inf_{(x, y) \sim \mathcal{D}} \mathcal{S}(\ell_{\mathcal{F}}, \ell_{\mathcal{G}}, x, y)$. Similar to Demontis *et al.* [9], we define the expected loss gradient similarity as $\tilde{\mathcal{S}}_{\mathcal{D}}(\ell_{\mathcal{F}}, \ell_{\mathcal{G}}) = \mathbb{E}_{(x, y) \sim \mathcal{D}} [\mathcal{S}(\ell_{\mathcal{F}}, \ell_{\mathcal{G}}, x, y)]$, which can capture the similarity between two models on \mathcal{D} . Naturally, a larger gradient similarity indicates a more general alignment between the adversarial directions of two given models. We can sample a set of data from \mathcal{S} to evaluate this alignment between two models on \mathcal{D} .

Definition 3 (Transferability). Given a normal sample $(x, y) \in \mathcal{D}$, and a perturbed version $x + \delta$ crafted against a surrogate model \mathcal{F} . The transferability T_r between \mathcal{F} and a target model \mathcal{G} is defined as $T_r = \mathbb{I}[\mathcal{F}(x) = \mathcal{G}(x) = y \wedge \mathcal{F}(x + \delta) \neq y \wedge \mathcal{G}(x + \delta) \neq y]$, where \mathbb{I} denotes the indicator function.

Here we define transferability the same way as [65] for untargeted attacks at the instance level. A successful untargeted

targeted transfer attack requires both the surrogate and the target models to give correct predictions for the unperturbed input and incorrect predictions for the perturbed one. The targeted version is similar. Note that we abuse the notations δ and ϵ in Definition 3 and Theorem 1, while the notations in Eq. (1) have similar meanings under different contexts.

Theorem 1 (Lower bound of transferability). Given any sample $(x, y) \in \mathcal{D}$, let $x + \delta$ denote a perturbed version of x with fooling probability $\Pr(\mathcal{F}(x + \delta) \neq y) \geq (1 - \alpha)$ and perturbation budget $\|\delta\|_2 \leq \epsilon$. Then the transferability $\Pr(T_r(\mathcal{F}, \mathcal{G}, x, y) = 1)$ between surrogate model \mathcal{F} and target model \mathcal{G} can be lower bounded by

$$\Pr(T_r(\mathcal{F}, \mathcal{G}, x, y) = 1) \geq \frac{(1 - \alpha) - (\gamma_{\mathcal{F}} + \gamma_{\mathcal{G}})}{\epsilon - c_{\mathcal{G}}} - \frac{\epsilon(1 - \alpha)}{\epsilon - c_{\mathcal{G}}} \frac{\sqrt{2 - 2\underline{\mathcal{S}}_{\mathcal{D}}(\ell_{\mathcal{F}}, \ell_{\mathcal{G}})}}{\sqrt{2 - 2\bar{\sigma}_{\mathcal{F}}\epsilon^2/2}},$$

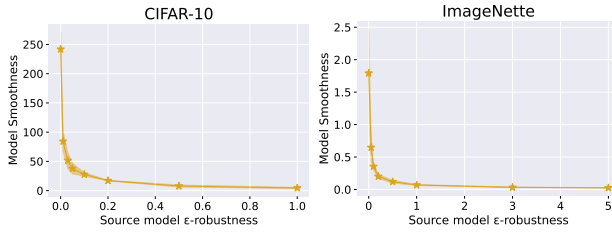
$$c_{\mathcal{F}} = \min_{(x, y) \sim \mathcal{D}} \frac{\min_{y' \in \mathcal{L}: y' \neq y} \ell_{\mathcal{F}}(x + \delta, y') - \ell_{\mathcal{F}}(x, y) - \bar{\sigma}_{\mathcal{F}}\epsilon^2/2}{\|\nabla_x \ell_{\mathcal{F}}(x, y)\|_2},$$

$$c_{\mathcal{G}} = \max_{(x, y) \sim \mathcal{D}} \frac{\min_{y' \in \mathcal{L}: y' \neq y} \ell_{\mathcal{G}}(x + \delta, y') - \ell_{\mathcal{G}}(x, y) + \bar{\sigma}_{\mathcal{G}}\epsilon^2/2}{\|\nabla_x \ell_{\mathcal{G}}(x, y)\|_2}. \quad (2)$$

The natural risks (inaccuracy) of models \mathcal{F} and \mathcal{G} on \mathcal{D} are defined as $\gamma_{\mathcal{F}}$ and $\gamma_{\mathcal{G}}$ respectively, and $\bar{\sigma}_{\mathcal{F}}$ and $\bar{\sigma}_{\mathcal{G}}$ are the upper smoothness of \mathcal{F} and \mathcal{G} .

Note that we deliver the lower bound of transferability for untargeted attacks as an example, and the targeted attack follows a similar form. The conclusions for the targeted attack agree with the untargeted case, as suggested in [65], so we omit it for space. The proof is provided in the Appendix. Although the theorem is initially for l_2 -norm perturbations, it can be generalized to l_{∞} -norm as demonstrated in [65].

Implications. Intuitively, we expect to enlarge the lower bound of transferability as much as possible. Different from [65], which seeks to suppress the transferability from both surrogate and target sides, this paper focuses on the surrogate aspect to increase transferability. Therefore, we next briefly analyze how all the terms relating to \mathcal{F} influence the lower bound.

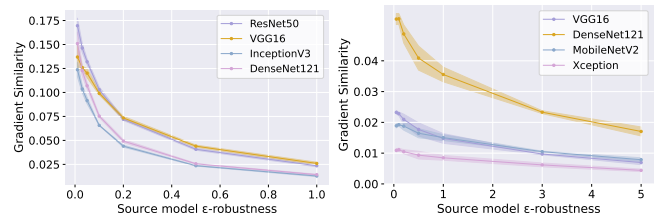


(a) ResNet18 on CIFAR-10 (b) ResNet50 on ImageNette

Figure 3: Average model smoothness of ϵ -robust models trained over 3 different random seeds with corresponding error bars at each ϵ . Note that the variances are very small.

- **fooling probability** $1 - \alpha$: this term captures the likelihood of the surrogate \mathcal{F} being fooled by the adversarial instance $x + \delta$. Different AEs generation strategies result in different fooling probabilities. Intuitively, if $x + \delta$ is unable to fool \mathcal{F} , we would expect it cannot fool \mathcal{G} as well. The theorem also suggests effective attack strategies to increase the lower bound. Therefore we default to using a strong baseline attack, projected gradient descent (PGD) (Tabs. II and XIII). We also report the results of AutoAttack (a gradient-based and gradient-free ensemble attack) in the Appendix (Tab. XII) to ensure the consistency of conclusions.
- **natural risk** $\gamma_{\mathcal{F}}$: the negative effect of natural risk on the lower bound of transferability is obvious. A model with lame accuracy on \mathcal{D} is certainly undesirable for adversarial attacks. Consequently, we minimize this term by training models with sufficient epochs for CIFAR-10 and fine-tuning pre-trained ImageNet classifiers for ImageNette.
- **gradient similarity** $\mathcal{S}_{\mathcal{D}}(\ell_{\mathcal{F}}, \ell_{\mathcal{G}})$: $\bar{\sigma}_{\mathcal{G}}$ is small compared with the perturbation radius ϵ , and the gradient magnitude $\|\nabla_x \ell_{\mathcal{G}}\|_2$ is relatively large, leading to a small $c_{\mathcal{G}}$. Additionally, $1 - \alpha$ is large since the attack is generally effective against \mathcal{F} . Thus, the right side of the inequality has a form of $C - k\sqrt{1 - \mathcal{S}_{\mathcal{D}}(\ell_{\mathcal{F}}, \ell_{\mathcal{G}})}$. Since C and k are both positive, there is a positive relationship between gradient similarity and the lower bound.
- **model smoothness** $\bar{\sigma}_{\mathcal{F}}$: It's obvious that a smaller $\bar{\sigma}_{\mathcal{F}}$ generates a larger $c_{\mathcal{F}}$, resulting in a larger lower bound. This indicates smoother models in the input space might serve as better surrogates for transfer attacks.

It is worth noting that a sensible adversary naturally desires to use more precise surrogates and stronger attacks against unknown targets. However, smoothness and similarity are more complex to understand and optimize compared to fooling probability and natural risk. Therefore, we focus on investigating the connection between smoothness, similarity, and transferability as well as how the various training mechanisms regulate them under the restriction that the other two factors above are fairly acceptable. Prior study [9] has shown their link with transferability separately, while we explore their joint effect on transferability.



(a) CIFAR-10 (b) ImageNette

Figure 4: Average gradient similarities between ϵ -robust models and different target models with corresponding error bars at each ϵ . We also report results over 3 different random seeds.

C. Transferability Circuit of Adversarial Training

Through a combination of theoretical analysis and experimental measurements, here we provide our insights into this “transferability circuit” in adversarial training. Arguably, we have the following two hypotheses.

From surrogate perspective, the trade-off between model smoothness and gradient similarity largely dictates adversarial transferability. First, through mathematical derivation and empirical results, we demonstrate that AT implicitly improves model smoothness. We rewrite the adversarial loss in Eq. (1) as: $\ell(f(x_i), y_i) + [\max_{\|\delta\|_2 \leq \epsilon} \ell(f(x_i + \delta), y_i) - \ell(f(x_i), y_i)]$. The latter term reflects the non-smoothness around point (x_i, y_i) . Assuming x_i is a local minimum of $\ell(f(\cdot), y_i)$ and applying a Taylor expansion, we get: $\max_{\|\delta\|_2 \leq \epsilon} \ell(f(x_i + \delta), y_i) - \ell(f(x_i), y_i) = \frac{1}{2}\sigma(\nabla x^2 \ell(f(x_i), y_i)) \cdot \|\delta\|_2^2 + O(\|\delta\|_2^3)$ since the first-order term is 0 at a local minimum. Therefore, AT implicitly penalizes the curvature of $\ell(f(x_i), y_i)$ with a penalty proportional to $\|\delta\|_2^2$.

Accordingly, a larger ϵ strengthens the effect of producing models with greater smoothness. Fig. 3 shows the mean dominant eigenvalues of the Hessian for AT models under various perturbation budgets. It reveals that AT consistently suppresses the dominant eigenvalue, stably producing smoother models. On the other hand, we also find that AT reduces gradient similarity. Fig. 4 shows the decrease in similarity between surrogate and target models as the budget increases. Notably, for each dataset, smoothness rapidly improves for small ϵ (as shown by the steep slope in Fig. 3), while gradient similarity gradually decreases. For larger ϵ , improvements in smoothness become marginal since the models are already very smooth. As a reminder, we have controlled the other two terms to be reasonably acceptable. These suggest that:

- The quick improvement in transferability for small ϵ occurs because of the rapid gains in smoothness and small decays in gradient similarity.
- The degradation in transferability for large ϵ occurs because smoothness gains have approached the limit while gradient similarity continues to decrease.

Based on the above analyses, we can infer that the “transferability circuit” of AT may primarily arise from the trade-off effect between smoothness and similarity, given the restriction

of surrogates with relatively good accuracies and a highly effective attack strategy. This inference is intuitively inspired by the implications regarding all the surrogate-related factors in Theorem 1.

Meanwhile, we observe that the “transferability circuit” of AT generally exists, though it varies under different non-surrogate circumstances. For example, the optimal ϵ AT to achieve the best ASRs varies among datasets and perturbation budgets in Fig. 2. This suggests that for different non-surrogate factors, the extent to which model smoothness and gradient similarity contribute to transferability may vary.

Consequently, we propose the hypothesis that when generating AEs against accurate surrogate models using effective strategies, the trade-off between model smoothness and gradient similarity is strongly correlated with the transferability of those examples from the surrogate models. To test this hypothesis, we will investigate changes in model smoothness and gradient similarity alongside the corresponding transfer ASRs under various surrogate training mechanisms in Secs. III and IV. Furthermore, in Sec. VI, Q1, we provide a statistical analysis of the correlations between model smoothness, gradient similarity and transferability. Moving forward, the primary concern at hand is to ascertain the rationale of this similarity deterioration in AT, as well as how to generally avoid this and reach a better balance of smoothness and similarity for stronger transfer attacks.

Data distribution shift impairs gradient similarity. Different from model smoothness, it is difficult to understand how exactly AT degrades the gradient similarity. In this work, we attribute the degradation to the data distribution shift induced by the off-manifold examples in AT. Since the emerging of adversarial examples [54], there is a long-held belief that: *Clean data lies in a low-dimensional manifold. Even though the adversarial examples are close to the clean data, they lie off the underlying data manifold* [20, 26, 33, 50]. Nevertheless, recent researches demonstrate that AEs can also be on-manifold [27, 30, 43, 53], and on-manifold and off-manifold AEs may co-exist [63]. With this in mind, we analyze how large-budget AT can induce more off-manifold training samples. Given a regular loss function $\ell(f(x), y)$ on the low-dimensional manifold \mathcal{M} , the adversarial perturbation $\delta \in \mathbb{R}^d$ could make the loss $\ell(f(x + \delta), y)$ sufficiently high with $x + \delta \in \mathcal{M}$ or $x + \delta \notin \mathcal{M}$. At a high level, AT augments the dataset by adding adversarial examples during each iteration, obtaining an augmented data distribution on $\mathcal{P}_{\mathcal{X}}$, and the adversarial budget ϵ can be regarded as a parameter that controls the augmentation magnitude. Intuitively, a larger ϵ induces a larger distribution shift, resulting in more space for off-manifold samples. Accordingly, a larger ϵ may cause more disbenefit of underfitting to normal \mathcal{M} . We formalize the second hypothesis as follows:

Hypothesis 1 (Distribution shift impairs gradient similarity). *Given two data distribution $\mathcal{D}, \mathcal{D}' \in \mathcal{P}_{\mathcal{X} \times \mathcal{Y}}$, and two source models $\mathcal{F}_{\mathcal{D}}$ and $\mathcal{F}_{\mathcal{D}'}$ trained on \mathcal{D} and \mathcal{D}' , respectively, supposing the target model $\mathcal{G}_{\mathcal{D}}$ is also trained on \mathcal{D} and they*

all share a joint training loss ℓ , if the distance between \mathcal{D} and \mathcal{D}' is large enough, then $\tilde{\mathcal{S}}_{\mathcal{D}}(\ell_{\mathcal{F}_{\mathcal{D}}}, \ell_{\mathcal{G}_{\mathcal{D}}}) < \tilde{\mathcal{S}}_{\mathcal{D}}(\ell_{\mathcal{F}_{\mathcal{D}'}, \ell_{\mathcal{G}_{\mathcal{D}}}})$ is likely to stand.

The intuition behind this hypothesis is that, on average, the two models trained on the same distribution should align better in the gradient direction than those trained with different distributions. Note that, we relax the distribution change of AT on $\mathcal{P}_{\mathcal{X}}$ to $\mathcal{P}_{\mathcal{X} \times \mathcal{Y}}$ here, hypothesizing the general change on $\mathcal{P}_{\mathcal{X} \times \mathcal{Y}}$ impairs gradient similarity.

III. THE TRADE-OFF UNDER DATA AUGMENTATION

To extend the distribution shifts of AT to more general cases and further verify Hypothesis 1, we investigate how data augmentations, the popular training paradigm that explicitly changes data distribution, influence gradient similarity. Additionally, we investigate the trade-off effect between similarity and smoothness under data augmentations and observe how they reflect on the transfer attack performance accordingly.

A. Data Augmentation Mechanisms

We visit 4 popular data augmentation mechanisms and choose proper augmentation magnitude parameters to control the degree of data distribution shift from \mathcal{D} to \mathcal{D}' , aligning the augmentation parameter ϵ in AT.

Mixup (MU) [68] trains a model on the convex combination of randomly selected sample pairs, *i.e.*, the mixed image $\tilde{x}_{i,j} = bx_i + (1 - b)x_j$ and the corresponding label $\tilde{y}_{i,j} = by_i + (1 - b)y_j$, where $(x_i, y_i), (x_j, y_j) \in \mathcal{S}$. Here $b \in [0, 1]$ is a random variable drawn from the Beta distribution Beta(1, 1). Additionally, we use a probability parameter \mathbf{p} to control how much \mathcal{D}' shifts away from \mathcal{D} . Specifically, as $\mathbf{p} \rightarrow 0$, the augmented dataset will be identical to \mathcal{S} ; as $\mathbf{p} \rightarrow 1$, all the samples will be interpolated. We train augmented models for MU with $\mathbf{p} \in [0.1, 0.3, 0.5, 0.7, 0.9]$.

Cutmix (CM) [67] also augments both images and labels by mixing samples. The difference is patches are cut and pasted among training samples. A mixed sample $\tilde{x}_{i,j} = \mathbf{M}_{\mathbf{b}} \odot x_i + (1 - \mathbf{M}_{\mathbf{b}}) \odot x_j$ and its label $\tilde{y}_{i,j}$ are also obtained from two samples $(x_i, y_i), (x_j, y_j) \in \mathcal{S}$, where $\mathbf{M}_{\mathbf{b}}$ is a binary matrix with the same size of x_i to indicate the location for cutting and pasting, $\mathbf{1}$ is a matrix filled with 1, and b is drawn from Beta(1, 1). Similar to MU, we use a probability parameter \mathbf{p} to control the augmentation magnitude and train augmented models for CM with $\mathbf{p} \in [0.1, 0.3, 0.5, 0.7, 0.9]$.

Cutout (CO) [10] augments the dataset by masking out random regions of images with a size less than $M \times M$. The parameter M controls the augmentation magnitude. We train augmented models for CO with $M \in [8, 12, 16, 20, 24]$ and $M \in [80, 100, 120, 140, 160]$ for CIFAR-10 and ImageNette, respectively.

Label smoothing (LS) [55] augments the dataset by replacing the hard labels \mathcal{L} with soft continuous labels in probability distribution. Specifically, the probability of the ground-truth class is $1 - p$, and the probability of other classes will be uniformly assigned to $p/(m - 1)$, where $p \in [0, 1]$ and m

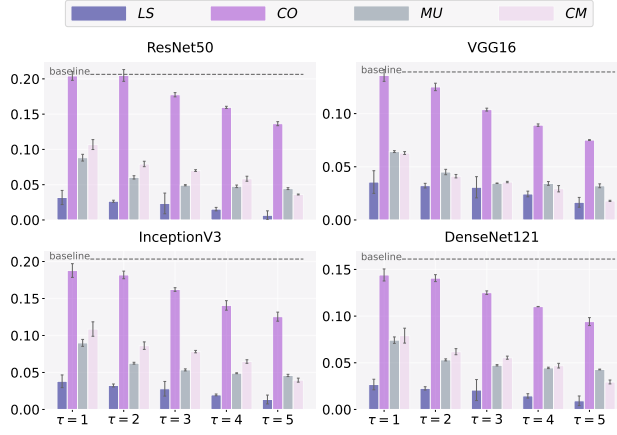


Figure 5: Average gradient similarities between augmented and target models on CIFAR-10 with error bars at each τ .

denotes the number of classes. We train models for LS with $p \in [0.1, 0.2, 0.3, 0, 4, 0.5]$.

These augmentations along with AT change data distributions in distinct manners. For a normal sample $(x, y) \sim \mathcal{D}$, AT associates input feature x with ground-truth y “inaccurately” under a noise δ , while CO associates part of “right” x with ground-truth y , thus they explicitly change the distribution on \mathcal{P}_x . Contrarily, both MU and CM correlate parts of x with y , causing shift in $\mathcal{P}_{x \times y}$. Whereas LS relates the full x to a “wrong” y' , causing shift in \mathcal{P}_y . Intuitively, these augmentation methods will cause different impacts on the gradient $\nabla \ell_{\mathcal{F}}(x, y)$. As we select 5 augmentation magnitudes for each augmentation, we use a general parameter $\tau \in [1, 2, 3, 4, 5]$ to simplify the notations, e.g., $\tau = 1$ means $p = 0.1$ for MU and $M = 8$ for CO on CIFAR-10.

B. Data Augmentation Impairs Gradient Similarity

To verify Hypothesis 1, we explore how different data distribution shifts influence gradient similarity. For all the experiments, we train models with 3 different random seeds in each setting. Besides, multiple target models are considered to ensure generality. The average results over 3 standard training (ST) models without augmentations are used as baselines.

Fig. 5 and Fig. 10 (moved to appendix) depict the alignments towards multiple target models for CIFAR-10 and ImageNette, respectively. First, we observe that CO harms gradient similarity the least, but its effect varies across different datasets. Specifically, CO slightly degrades gradient similarity in CIFAR-10, while appearing comparable to baselines in ImageNette. The gap between the two datasets can be attributed to different training settings. CIFAR-10 models are trained from scratch, while ImageNette models are obtained by fine-tuning well-trained ImageNet classifiers. ImageNette is a 10-class subset of ImageNet, which suggests that merely cutting part of the pixels does not suffice to make the model forget what it “see” before. On the other hand, LS , MU , and CM degrade similarity largely over both datasets. Note that the similarity degradation of these augmentations is in line with

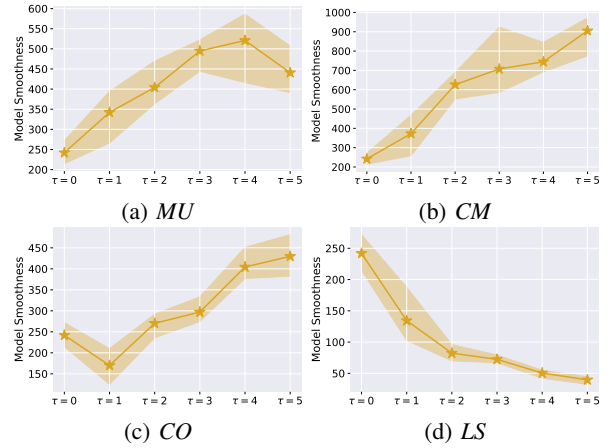


Figure 6: Average model smoothness of augmented models on CIFAR-10 with respective error bars at each τ .

their manipulations on \mathcal{P}_y , suggesting modifying the ground-truth y during training results in more impacts on the direction of gradient $\nabla \ell_{\mathcal{F}}(x, y)$. In summary, despite subtle differences, the results on both datasets confirm our hypothesis, and the distribution change of \mathcal{P}_y could have more negative impacts on gradient similarity than that of \mathcal{P}_x .

C. Transferability Trade-off Under Data Augmentation

To figure out how these augmentations influence smoothness and transferability, we measure smoothness and the consequent ASRs of AEs w.r.t. these augmented models. To save space, we merely report the $\tau = 1, 5$ cases for PGD attack in Tabs. II and XIII, as they represent the smallest and largest augmentation magnitudes. We report the $\tau = 1, 3, 5$ cases for AutoAttack in Tab. XII. Figs. 6 and 9 plot the smoothness for two datasets.

First, LS exhibits a monotonous benefit on smoothness on both datasets due to its implicit effect on reducing the gradient norm during training [55]. However, the tables show that the ASRs of LS are always lower than those of ST , implying this benefit may not completely offset the negative effect of largely degraded similarity in LS . Additionally, there is no monotonicity in ASRs in LS , aligning with the always combating negative and positive effects. In contrast, other augmentations do not exhibit a consistent tendency for smoothness on both datasets. Specifically, in CIFAR-10, CM , MU , and CO mostly degrade the smoothness while the degradation is not strictly monotonous. The situation is even more chaotic in ImageNette, where the variances of smoothness are relatively large. However, the ASRs do reveal some patterns. For CM and MU , their ASRs degrade from $\tau = 1$ to $\tau = 5$, and the ASRs of CO are generally better than MU and CM . Notably, CO performs slightly better than ST under a few cases, especially when $\tau = 1$. This agrees with the fact that CO has slightly better smoothness and less severely degraded similarity. Conclusively, the trade-off under data augmentations is quite complex, and no single augmentation can generally produce good surrogates.

TABLE II: Untargeted and targeted transfer ASRs of AEs crafted against baseline (*ST*), data augmentations, adversarial training, and gradient regularizations surrogates under the different L_∞ budgets (4/255, 8/255, 16/255) on **CIFAR-10** using **PGD**. Results in gray are (more than 0.2%) below the baseline, results in white are close to the baseline ($\pm 0.2\%$). Results in darkest orange are the highest in each respective column, the second darkest are the second highest, and the least dark are others more than 0.2% above the baseline. We conduct experiments using surrogate models trained from 3 different random seeds in each setting and report the average results and the according error bars. In %.

	Untargeted											
	4/255				8/255				16/255			
	ResNet50	VGG16	InceptionV3	DenseNet121	ResNet50	VGG16	InceptionV3	DenseNet121	ResNet50	VGG16	InceptionV3	DenseNet121
<i>ST</i>	54.3 \pm 2.9	42.3 \pm 1.9	53.6 \pm 2.3	70.7 \pm 2.0	79.9 \pm 3.4	71.4 \pm 3.5	80.1 \pm 3.2	93.0 \pm 1.2	92.8 \pm 1.6	90.6 \pm 1.9	93.3 \pm 2.2	98.6 \pm 0.5
<i>MU</i> , $\tau = 1$	34.7 \pm 2.6	26.7 \pm 1.1	35.8 \pm 1.8	47.1 \pm 3.0	57.1 \pm 3.6	49.1 \pm 2.2	59.2 \pm 2.6	74.0 \pm 2.8	76.6 \pm 4.1	75.2 \pm 3.4	79.9 \pm 2.5	90.2 \pm 2.4
<i>MU</i> , $\tau = 5$	18.5 \pm 0.5	15.5 \pm 0.2	19.6 \pm 0.3	22.8 \pm 0.5	31.3 \pm 1.7	27.6 \pm 0.7	34.5 \pm 0.7	40.7 \pm 1.2	49.9 \pm 1.5	49.1 \pm 0.9	54.4 \pm 0.3	62.8 \pm 1.2
<i>CM</i> , $\tau = 1$	29.3 \pm 1.2	21.3 \pm 0.5	28.4 \pm 2.1	39.8 \pm 2.0	46.4 \pm 2.5	37.6 \pm 1.4	45.6 \pm 3.2	62.8 \pm 2.4	63.3 \pm 2.6	60.2 \pm 1.4	63.9 \pm 3.2	81.1 \pm 1.2
<i>CM</i> , $\tau = 5$	13.5 \pm 0.3	10.8 \pm 0.1	13.1 \pm 0.4	15.1 \pm 0.3	19.5 \pm 0.4	15.7 \pm 0.2	18.7 \pm 0.8	22.6 \pm 0.7	29.4 \pm 1.4	28.6 \pm 1.0	29.3 \pm 1.1	34.3 \pm 1.5
<i>CO</i> , $\tau = 1$	51.5 \pm 2.3	41.3 \pm 2.4	50.0 \pm 1.8	67.7 \pm 1.4	78.7 \pm 2.4	71.9 \pm 3.2	78.2 \pm 0.9	92.3 \pm 0.9	93.0 \pm 2.1	91.8 \pm 1.5	93.6 \pm 0.7	98.9 \pm 0.2
<i>CO</i> , $\tau = 5$	37.7 \pm 2.8	26.9 \pm 1.7	36.9 \pm 2.0	49.5 \pm 1.2	63.9 \pm 4.5	53.1 \pm 3.6	64.1 \pm 3.9	80.4 \pm 1.1	84.7 \pm 3.3	79.1 \pm 3.5	85.5 \pm 3.2	95.3 \pm 1.0
<i>LS</i> , $\tau = 1$	33.4 \pm 1.7	28.6 \pm 1.4	33.2 \pm 0.6	43.4 \pm 1.5	47.5 \pm 2.0	44.8 \pm 1.1	47.6 \pm 0.8	61.8 \pm 1.9	59.9 \pm 1.5	63.0 \pm 1.1	62.9 \pm 1.0	75.8 \pm 1.4
<i>LS</i> , $\tau = 5$	32.8 \pm 0.5	28.0 \pm 1.3	31.9 \pm 0.7	40.8 \pm 1.8	50.7 \pm 1.4	46.8 \pm 2.4	50.6 \pm 0.6	63.4 \pm 0.9	65.3 \pm 2.1	66.1 \pm 1.9	66.7 \pm 0.5	78.0 \pm 0.7
<i>AT</i>	59.0 \pm 3.0	50.3 \pm 4.4	53.3 \pm 2.9	65.3 \pm 2.7	87.8 \pm 2.8	82.7 \pm 4.5	84.7 \pm 2.7	92.2 \pm 0.8	96.9 \pm 1.3	95.8 \pm 2.0	96.0 \pm 1.4	98.6 \pm 0.3
<i>IR</i>	62.3 \pm 1.2	55.6 \pm 0.5	56.5 \pm 2.1	63.7 \pm 1.9	96.0 \pm 0.4	93.2 \pm 0.2	93.8 \pm 0.6	96.9 \pm 0.6	99.9 \pm 0.0	99.7 \pm 0.0	99.8 \pm 0.1	99.9 \pm 0.1
<i>JR</i>	74.2 \pm 2.0	65.8 \pm 0.8	72.6 \pm 0.3	84.1 \pm 0.5	94.1 \pm 0.7	91.3 \pm 0.3	93.4 \pm 0.6	97.7 \pm 0.5	98.3 \pm 0.3	98.3 \pm 0.2	98.5 \pm 0.4	99.7 \pm 0.5
<i>ER</i>	64.9 \pm 3.3	52.5 \pm 1.9	54.2 \pm 6.7	62.8 \pm 10.9	94.2 \pm 1.4	87.1 \pm 5.3	87.9 \pm 4.7	92.8 \pm 5.3	99.6 \pm 0.2	98.7 \pm 4.0	98.6 \pm 0.8	99.5 \pm 0.6
<i>SAM</i>	76.1 \pm 1.5	64.3 \pm 2.1	74.5 \pm 0.7	88.5 \pm 0.4	97.5 \pm 0.5	94.1 \pm 0.8	97.1 \pm 0.1	99.6 \pm 0.1	99.8 \pm 0.0	99.7 \pm 0.1	99.9 \pm 0.0	100.0 \pm 0.0
<i>SAM&IR</i>	64.7 \pm 0.3	58.2 \pm 0.4	58.4 \pm 1.6	65.4 \pm 1.0	97.6 \pm 0.0	95.5 \pm 0.1	95.9 \pm 0.4	97.9 \pm 0.3	100.0 \pm 0.0	99.9 \pm 0.0	100.0 \pm 0.0	100.0 \pm 0.0
<i>SAM&JR</i>	83.1 \pm 0.6	70.1 \pm 0.9	79.4 \pm 0.6	91.5 \pm 0.3	98.6 \pm 0.2	96.6 \pm 0.2	98.3 \pm 0.1	99.9 \pm 0.0	99.9 \pm 0.0	99.9 \pm 0.0	99.9 \pm 0.0	100.0 \pm 0.0
	Targeted											
	18.3 \pm 1.4	12.7 \pm 0.6	20.4 \pm 1.1	34.9 \pm 1.9	39.4 \pm 4.9	32.7 \pm 3.6	43.6 \pm 4.0	68.8 \pm 4.0	55.7 \pm 6.0	53.5 \pm 5.5	60.0 \pm 5.3	85.4 \pm 4.2
	8.2 \pm 0.8	5.9 \pm 0.5	10.5 \pm 0.6	15.9 \pm 1.0	17.0 \pm 2.7	13.8 \pm 1.4	20.7 \pm 2.1	33.3 \pm 3.5	28.0 \pm 5.1	26.8 \pm 2.9	33.1 \pm 3.5	50.9 \pm 6.2
	3.0 \pm 0.1	2.4 \pm 0.1	4.1 \pm 0.1	5.0 \pm 0.2	6.1 \pm 0.5	5.0 \pm 0.4	7.9 \pm 0.5	10.4 \pm 0.5	10.8 \pm 0.5	10.7 \pm 0.6	13.5 \pm 0.6	16.9 \pm 0.9
	6.0 \pm 0.4	4.2 \pm 0.2	6.8 \pm 1.0	11.4 \pm 1.1	10.7 \pm 0.7	8.3 \pm 0.5	11.6 \pm 1.8	20.8 \pm 1.9	16.4 \pm 0.9	14.9 \pm 0.8	17.3 \pm 2.5	29.6 \pm 1.7
	2.0 \pm 0.1	1.6 \pm 0.1	2.4 \pm 0.2	2.8 \pm 0.2	2.8 \pm 0.1	2.3 \pm 0.0	3.2 \pm 0.1	3.7 \pm 0.1	4.2 \pm 0.2	3.9 \pm 0.4	4.4 \pm 0.2	4.7 \pm 0.3
	16.0 \pm 1.3	11.3 \pm 1.2	17.6 \pm 1.1	30.6 \pm 1.7	35.8 \pm 3.0	30.7 \pm 2.5	38.6 \pm 2.7	63.4 \pm 2.2	52.8 \pm 4.3	51.5 \pm 3.0	55.9 \pm 3.1	82.1 \pm 1.6
	7.9 \pm 1.1	5.4 \pm 0.5	9.5 \pm 0.7	14.2 \pm 0.7	17.4 \pm 2.9	13.6 \pm 1.3	20.5 \pm 2.1	31.1 \pm 0.9	29.1 \pm 5.0	24.9 \pm 2.8	31.9 \pm 4.1	48.5 \pm 1.8
	6.8 \pm 0.6	5.4 \pm 0.4	7.0 \pm 0.3	10.7 \pm 1.3	9.9 \pm 3.8	9.0 \pm 4.0	10.0 \pm 3.3	15.6 \pm 6.2	15.4 \pm 1.9	16.7 \pm 1.8	16.3 \pm 1.2	23.9 \pm 2.9
	6.7 \pm 0.4	5.7 \pm 0.1	7.1 \pm 0.8	10.5 \pm 1.3	13.5 \pm 1.1	12.8 \pm 0.7	14.0 \pm 1.5	20.1 \pm 2.0	19.4 \pm 0.9	20.0 \pm 0.3	20.0 \pm 1.4	27.0 \pm 1.8
	24.9 \pm 2.2	18.6 \pm 3.4	21.9 \pm 2.0	32.5 \pm 2.5	60.7 \pm 6.7	52.4 \pm 7.9	55.6 \pm 5.5	72.6 \pm 4.0	77.4 \pm 7.7	74.6 \pm 7.9	72.4 \pm 6.7	88.4 \pm 4.1
	25.7 \pm 1.1	20.6 \pm 0.2	22.5 \pm 1.1	28.8 \pm 1.3	70.8 \pm 0.5	62.8 \pm 0.7	65.0 \pm 1.5	75.2 \pm 0.6	89.9 \pm 0.7	86.7 \pm 0.8	86.3 \pm 1.3	92.7 \pm 0.8
	38.6 \pm 2.6	30.3 \pm 1.2	39.1 \pm 0.1	54.0 \pm 1.2	75.2 \pm 3.9	69.6 \pm 2.5	76.0 \pm 0.9	90.0 \pm 0.8	87.3 \pm 2.8	88.9 \pm 1.8	88.4 \pm 1.0	97.6 \pm 0.3
	22.7 \pm 1.6	15.5 \pm 2.8	17.8 \pm 3.4	24.1 \pm 8.1	54.6 \pm 3.3	42.7 \pm 6.9	44.1 \pm 8.0	55.0 \pm 15.9	77.2 \pm 3.0	67.2 \pm 8.3	66.5 \pm 9.6	76.6 \pm 16.7
	35.0 \pm 1.9	25.2 \pm 1.8	36.9 \pm 1.3	56.7 \pm 0.2	74.7 \pm 3.1	65.7 \pm 3.5	76.5 \pm 1.9	94.0 \pm 0.4	92.3 \pm 1.5	90.9 \pm 2.2	93.4 \pm 0.3	99.5 \pm 0.2
	28.6 \pm 0.2	23.5 \pm 0.2	25.0 \pm 1.2	31.4 \pm 0.7	81.8 \pm 0.0	75.7 \pm 0.2	77.6 \pm 1.1	84.8 \pm 0.6	99.2 \pm 0.1	98.7 \pm 0.1	98.6 \pm 0.4	99.6 \pm 0.1
	44.2 \pm 1.5	32.9 \pm 1.1	46.1 \pm 1.3	65.7 \pm 0.3	85.5 \pm 1.4	77.6 \pm 1.7	87.3 \pm 1.4	97.6 \pm 0.1	98.3 \pm 0.5	97.5 \pm 0.4	98.6 \pm 0.4	99.9 \pm 0.0

IV. THE TRADE-OFF UNDER GRADIENT REGULARIZATION

At present, we recognize what may harm gradient similarity, but have no idea of how to generally improve it. Additionally, it is challenging to regulate similarity independently without affecting other factors, especially in black-box scenarios where target models are unknown. In contrast, the standalone model smoothness can be regulated and measured with the surrogate itself. Therefore, we will explore how gradient regularization, which is expected to improve smoothness without changing the data distribution, can be used to enhance surrogates.

A. Gradient Regularization Mechanisms

We first formally define gradient regularization and deliver the intuitions on why they are chosen. To sharpen the analysis, we introduce the notation θ to parameterize a neural network and reform $f(\cdot)$ as $f_\theta(\cdot)$ if needed. For concise illustrations, we sometimes abbreviate $l(f(x), y)$ as $l(f(x))$ in this section.

1) *Regularization in the Input Space*: Based on the implication that regularizing input space smoothness benefits transferability shown in Sec. II-B, one should directly optimize

the loss surface curvature. However, it is challenging to realize it since the computationally expensive second-order derivative is involved, *i.e.*, $\nabla_x^2 \ell(f_\theta(x))$. Fortunately, deep learning and optimization theory [15] allow us to use the first-order derivative to approximate it. We thus choose two well-known first-order gradient regularizations as follows:

Input gradient regularization (*IR*): The Euclidean norm of gradient *w.r.t.* input x is added to the loss function in *IR* as:

$$L_{ir} = \frac{1}{\|\mathbf{S}\|} \sum_{i=1}^{\|\mathbf{S}\|} [\ell(f(x_i)) + \lambda_{ir} \|\nabla_x \ell(f(x_i))\|],$$

where λ_{ir} controls the regularization magnitude. *IR* has been demonstrated to be able to improve the generalization and interpretability of DNNs [15, 45]. *IR* has been demonstrated to be able to improve the generalization and robustness of neural networks [15, 45]. This is straightforward since *IR* directly penalizes solutions that are sensitive to the rate of change *w.r.t.* input features. Here we point out that *IR* actually has another underlying nature of benefiting adversarial transfer-

ability. That is, regularizing $\|\nabla_x \ell(f(x))\|_2$ leads to a smaller curvature $\sigma(\nabla_x^2 \ell(x))$ because the spectral norm of a matrix is upper-bounded by the Frobenius norm, *i.e.*, $\sigma(\nabla_x^2 \ell(x)) \leq \|\nabla_x^2 \ell(x)\|_F \approx \|\nabla_x \ell(f(x))^T \nabla_x \ell(f(x))\|_F \leq \|\nabla_x \ell(f(x))\|^2$. Note that here we approximate the second-order derivative using the first-order derivative as suggested in [24, 37]. Consequently, a smaller $\sigma(\nabla_x^2 \ell(x))$ indicates better smoothness, thereby improving transferability.

Input Jacobian regularization (JR): *JR* is mildly different than *IR*, as it regularizes the gradient on the logits output of the neural network as:

$$L_{jr} = \frac{1}{\|\mathbf{S}\|} \sum_{i=1}^{\|\mathbf{S}\|} [\ell(f_\theta(x_i) + \lambda_{jr} \|\nabla_x f_\theta(x_i)\|_F)].$$

JR has been also correlated with the enhanced generalization and adversarial robustness [4, 23, 24, 49, 57, 66]. Since *JR* has a similar form with *IR*, it is reasonable to presume that they have a similar effect. Formally, we prove that when $\|\nabla_x f_\theta(x_i)\|_F \rightarrow 0$, we have $\|\nabla_x \ell(f_\theta(x_i))\| \rightarrow 0$ using cross-entropy loss as an example (see Proposition 1 in the Appendix). This implies that *JR* also has a positive effect on model smoothness.

2) *Regularization in the Weight Space:* Recently, researchers paid attention to the gradient regularization on θ , *i.e.*, the parameters (weights) of the network. A recent study [11] proved that the gradient regularizing pressure on the weight space $\|\nabla_\theta f_\theta(x)\|_F$ can indeed transfer to the input space $\|\nabla_x f_\theta(x)\|_F$. Consequently, regularizing gradients *w.r.t.* the weight space could also promote the model smoothness in the input space in an implicit way. We next explore two representative weight gradient regularization methods as follows:

Explicit gradient regularization (ER): In *ER*, the Euclidean norm of gradient *w.r.t.* θ is added to the training loss L_{er} to promote flatness as:

$$L_{er}(\theta) = L(\theta) + \frac{\lambda_{er}}{2} \|\nabla_\theta L(\theta)\|^2,$$

where L is the original objective function. Similar to *IR* and *JR*, we can directly apply the double-propagation technique to implement the regularization term, using the automatic differentiation framework provided by modern ML libraries like PyTorch [42]. *ER* recently has been empirically shown to be able to improve generalization [3, 19, 48], while we study it from the transferability perspective.

Sharpness-aware minimization (SAM): *SAM* also seeks flat solution in the weight space. Specifically, it intends to minimize the original training loss and the worst-case sharpness $L_{sam}(\theta) = L(\theta) + [\max_{\|\hat{\theta} - \theta\|_2 \leq \rho} L(\hat{\theta}) - L(\theta)] = \max_{\|\hat{\theta} - \theta\|_2 \leq \rho} L(\hat{\theta})$, where ρ denotes the radius to search for the worst neighbor $\hat{\theta}$. As the exact worst neighbor is difficult to track, *SAM* uses the gradient of ascent direction neighbor for the update after twice approximations:

$$\nabla_\theta L_{sam}(\theta) \approx \nabla_\theta L(\theta + \rho \frac{\nabla_\theta L(\theta)}{\|\nabla_\theta L(\theta)\|}).$$

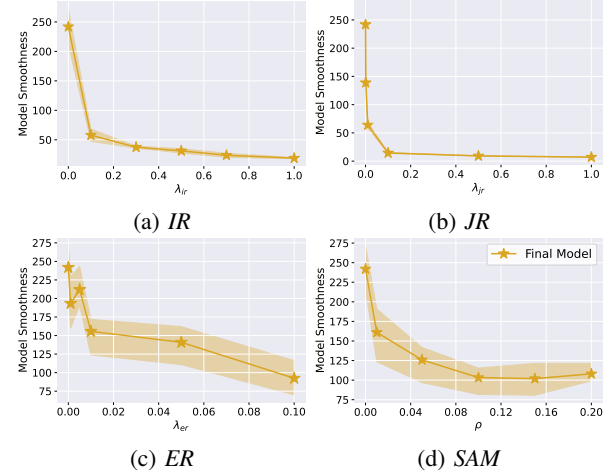


Figure 7: Average model smoothness of CIFAR-10 regularized (and *ST*) models. We trained 3 models using different random seeds for each setting to deliver average results. The standard accuracy of these models ranges from 90.12% to 95.38%.

Recent researches establish *SAM* as a special kind of gradient normalization [25, 69], where ρ represents the regularization magnitude. *SAM* has been extensively studied recently for its remarkable performance on generalization [1, 2, 6, 16, 17, 32, 38, 59, 71, 72]. In this paper, for the first time, we substantiate that *SAM* also features outstanding superiority in boosting transferability.

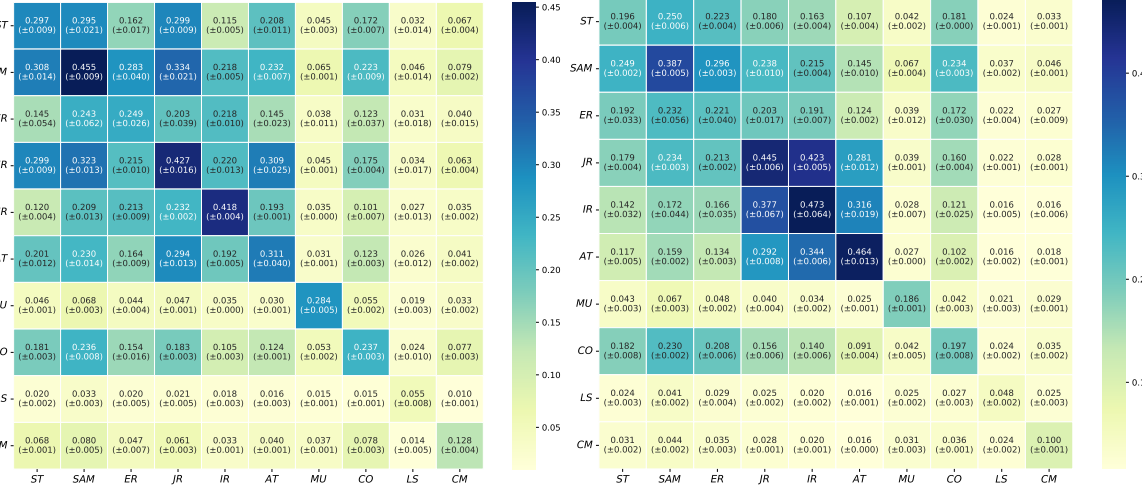
B. Gradient Regularization Promotes Model Smoothness

We train multiple regularized models for each regularization, and use coarse-grained parameter intervals [17, 45, 48] and restrict the largest regularized magnitude to avoid excessive regularization such that the accuracy of these models are above 90%. This allows for a fair comparison of each regularization method in an acceptable accuracy range. We choose 5 parameters in each interval through random grad and binary choices (See Tab. IX).

Figs. 7 and 11 depict the experimental results. We can observe regularization generally results in smoother models (*i.e.*, smaller smoothness values) than the baseline where the regularization magnitude is 0 (*ST*), and large magnitudes correspond to better smoothness. Moreover, input gradient regularization yields much better smoothness than weight gradient regularization, especially on CIFAR-10. This indicates that the transfer effect from weight space to input space suggested in [11] does exist, yet is somewhat marginal and cannot outperform direct regularizations in input space.

C. Transferability Trade-off Under Gradient Regularization

One might presume that input gradient regularization should clearly outperform weight gradient regularization in terms of transferability, which agrees with the conclusion that less complexity should exhibit better transferability in Demontis *et al.* [9], given that smoothness is positively correlated to the model complexity concept (as analyzed in Sec. VI, Q3). To



(a) ResNet18 trained over CIFAR-10

(b) ResNet50 trained over ImageNette

Figure 8: **Intra-architecture** gradient similarity between different mechanisms. Each cell reports the average result of 3 unique source-target pairs while each pair of models are trained with different random seeds, hence each matrix is asymmetric.

verify this, the average transfer ASRs of AEs crafted against these gradient regularized surrogates (from Figs. 7 and 11) are evaluated and reported in Tabs. II and XIII. The results show that *IR* and *JR* outperform *SAM* and *ER* in terms of ASRs on ImageNette. However, on CIFAR-10, *SAM* generally performs the best in terms of ASRs, despite yielding far worse smoothness than *IR* and *JR*. This finding not only weakens the conclusion in Demontis *et al.* [9], but also suggests an overall examination of these training mechanisms for superior surrogates, as they may weigh differently on gradient similarity.

V. BOOSTING TRANSFERABILITY WITH BETTER SURROGATES

Although we have concluded that gradient regularization can generally improve smoothness, the intangible nature of gradient similarity towards unknown target models still makes it difficult to guide us in obtaining better surrogates. We thus propose a general solution that can simultaneously improve smoothness and similarity, under a strict black-box scenario where target models are inaccessible. Our strategy involves first examining the pros and cons of various training mechanisms *w.r.t.* smoothness and similarity, and then combining their strengths to train better surrogates.

While gradient similarity cannot be directly measured when target models are unknown, one can assess the similarity between all the training mechanisms under the intra-architecture case. This helps to draw general conclusions that can be extended to the cross-architecture case as the angles between gradient directions follow the *triangle inequality*. Therefore, we measure the similarity between the surrogates we obtained thus far and report it in Fig. 8. And further results reported at Tab. VI in Sec. VI, Q2 can support the consistency posteriorly with observations in the cross-architecture case.

As a result, we obtain surrogates with superior smoothness and similarity, and extensive experiments demonstrate such cases where the trade-off is well reconciled superiorly improve the transferability.

A. A General Route for Constructing Better Surrogates

We first elaborate on some general observations about gradient regularization mechanisms as follows:

- **Input regularizations stably yield the best smoothness.** Figs. 7 and 11 show that *IR* and *JR* yield superior smoothness and their variances are small. This does not hold for other smoothness-benefiting mechanisms like *SAM*, *ER*. Further, Fig. 8 suggests that *IR*, *JR*, and *AT* align superiorly well with each other, this could be attributed to the fact that they all have a direct penalty effect on the input space, as analyzed in Secs. II-C and IV-A1.
- ***SAM* yields the best gradient alignments when input regularizations are not involved.** Fig. 8 shows that *SAM* exclusively exhibits better alignment towards every mechanism than *ST*. However, other mechanisms do not exhibit this advantage. Furthermore, if we exclude the diagonal elements, we can find *SAM* yields the best gradient similarity in each row and column except for the cases of *IR*, *JR*, and *AT*. This suggests that *SAM* has an underlying benefit on gradient similarity, which all the other mechanisms do not hold. We defer the detailed analysis on this to Sec. VI, Q7.
- **No single mechanism can dominate both datasets.** From Tabs. II and XIII, we observe that *SAM* yields the best ASRs on average on CIFAR-10. However, it generally performs worse than *IR* and *JR* on ImageNette. *ER*, on the other hand, consistently performs the worst on two datasets. Apparently, there is no one mechanism that can adequately outperform the others on both datasets.

TABLE III: Untargeted and targeted transfer ASRs when incorporating AE generation strategies under the different L_∞ budgets on CIFAR-10. Corresponding results are different from those of Tab. II due to different seeds of models. In %.

	Untargeted					Targeted										
	4/255		8/255			4/255		8/255								
	Res-50 VGG16 Inc-V3 Dense-121															
<i>ST</i>	55.94	42.48	53.89	71.64	79.77	70.83	78.85	93.05	19.92	12.97	20.71	37.01	44.11	35.37	46.59	73.56
<i>SAM</i>	75.45	61.65	75.51	88.44	96.97	92.85	96.84	99.63	35.63	24.69	40.51	59.50	74.05	64.04	79.49	94.30
<i>SAM&JR</i>	81.92	70.68	80.04	91.14	98.74	96.71	98.30	99.88	45.71	34.07	47.39	65.44	86.83	79.28	88.74	97.54
<i>ST+MI</i>	58.51	43.37	57.01	77.10	81.41	73.01	81.38	94.93	22.49	14.62	25.06	47.44	44.49	37.71	48.03	77.62
<i>SAM+MI</i>	80.53	65.02	80.54	92.54	97.58	93.82	97.71	99.75	44.12	29.69	50.12	72.37	81.34	73.18	85.56	97.11
<i>SAM&JR+MI</i>	85.35	73.83	83.77	93.72	98.94	97.13	98.68	99.85	54.38	39.86	55.68	74.87	91.15	84.44	92.66	98.63
<i>ST+DIM</i>	73.55	60.74	70.82	86.66	92.93	89.30	92.06	98.52	38.38	28.41	40.01	61.19	71.05	67.61	73.68	92.77
<i>SAM+DIM</i>	85.23	73.51	83.99	93.96	99.18	97.46	99.89	99.89	51.98	38.37	55.52	73.67	90.49	84.9	92.54	98.68
<i>SAM&JR+DIM</i>	85.14	75.73	83.13	92.65	99.42	98.43	99.08	99.89	55.48	43.07	55.61	72.15	94.40	89.78	94.37	98.89

TABLE IV: Transfer ASRs of AEs crafted against single and LGV ensemble surrogates under the different L_∞ budgets on CIFAR-10. Every single surrogate is used for baseline and compared with LGV ensemble of different fine-tuning strategies. We highlight the best ASRs in bold and those lower than baselines in red for each comparison. In %.

	Untargeted					Targeted										
	4/255		8/255			4/255		8/255								
	Res-50 VGG16 Inc-V3 Dense-121															
<i>ST</i>	55.94	42.48	53.89	71.64	79.77	70.83	78.85	93.05	19.92	12.97	20.71	37.01	44.11	35.37	46.59	73.56
<i>ST+LGV_{SGD}</i>	78.04	64.11	76.50	90.61	98.97	96.83	98.91	99.89	35.70	24.76	36.77	57.49	80.25	69.97	81.13	96.52
<i>ST+LGV_{SAM}</i>	83.75	70.12	81.44	93.75	99.60	98.11	99.36	99.95	44.66	30.17	45.47	67.93	90.64	81.86	90.87	98.75
<i>ST+LGV_{SAM&JR}</i>	83.63	70.12	81.87	93.52	99.28	97.33	99.06	99.96	46.14	31.85	47.66	68.72	89.67	80.43	90.06	98.54
<i>SAM</i>	75.45	61.65	75.51	88.44	96.97	92.85	96.84	99.63	35.63	24.69	40.51	59.50	74.05	64.04	79.49	94.30
<i>SAM+LGV_{SGD}</i>	69.09	54.31	70.63	85.04	92.14	84.70	92.57	98.74	28.55	18.60	33.58	53.21	59.12	48.21	65.60	87.95
<i>SAM+LGV_{SAM}</i>	82.13	69.01	82.54	93.20	99.13	97.38	99.13	99.92	42.83	29.14	47.46	67.11	87.54	79.35	91.09	98.44
<i>SAM+LGV_{SAM&JR}</i>	83.02	70.00	82.51	93.40	99.18	97.24	99.15	99.93	44.82	31.82	49.61	69.09	87.43	79.11	91.06	98.48
<i>SAM&JR</i>	81.92	70.68	80.04	91.14	98.74	96.71	98.30	99.88	45.71	34.07	47.39	65.44	86.83	79.28	88.74	97.54
<i>SAM&JR+LGV_{SGD}</i>	75.71	62.37	75.05	88.55	95.69	90.62	95.58	99.36	38.64	27.47	41.70	61.49	75.22	66.36	79.44	94.67
<i>SAM&JR+LGV_{SAM}</i>	83.20	71.74	81.97	92.88	99.16	97.40	99.06	99.92	45.34	33.40	47.73	67.24	88.72	80.86	90.63	98.37
<i>SAM&JR+LGV_{SAM&JR}</i>	84.86	73.37	83.32	93.52	99.51	98.11	99.28	99.94	49.07	36.04	51.37	70.79	90.61	83.50	92.36	98.70

The above observations inspire us that *SAM* and input regularization are highly complementary, and a straightforward solution to reach a better trade-off between model smoothness and gradient similarity is combining *SAM* with input gradient regularization, namely *SAM&IR* or *SAM&JR*. In other words, we believe *SAM&IR* and *SAM&JR* will bring significant improvement in transferability. To validate this, we conduct experiments on both CIFAR-10 and ImageNette, the results are also reported in Tabs. II and XIII for comparison. We can see that *SAM&JR* and *SAM&IR* generally perform the best in both datasets. Notably, we do not limit the route of constructing better surrogates to *SAM&IR* or *SAM&JR*, since there may exist other effective combinations or approaches as long as the trade-off between smoothness and similarity is well reconciled.

B. Incorporating Surrogate-independent Methods

We show that the surrogates obtained from our method (*e.g.*, *SAM* and *SAM&JR*) can be integrated with existing surrogate-independent methods to further improve transferability.

Incorporating AE generation strategies. Exploiting the generation process of AEs is a popular approach to improve transferability. The most representative methods include *momentum iterative* (MI) [12] and *diversity iterative* (DI) [64], and DI is frequently combined with MI and serves as a stronger baseline—*diversity iterative with momentum* (DIM). Generally, these designs are interpreted as constructing adversarial

examples that are less likely to fall into a poor local optimum of the given surrogate. Thus they adjust the update direction with momentum to escape it or apply multiple transformations on inputs to mimic an averagely flat landscape. We conduct experiments to verify that obtaining a better surrogate, which features less and wider local optima (analyzed in Sec. VI, Q3) and general adversarial direction, can further enhance these designs by promoting a larger lower bound.

In Tab. III, we report transfer ASRs using different generation strategies (PGD, MI, or DIM). The results show that using better surrogates can always significantly boost transferability. This suggests that the optima found in *ST* are inherently poorer than those in *SAM* and *SAM&JR*. Besides, without MI or DIM, *SAM&JR* using standard PGD alone already outperforms *ST+MI* and *ST+DMI*, implying that the lower bound of transferability of a better surrogate is sufficiently high, and may even surpass the upper bound of a poor model.

Incorporating ensemble strategies. Using multiple surrogates is widely believed to be able to update adversarial examples in a more general direction that benefits transferability. Recently, [21] proposed constructing the ensemble from a *large geometric vicinity* (LGV), *i.e.*, first fine-tuning a normally trained model with a high constant learning rate to obtain a set of intermediate models that belongs to a large vicinity, then optimizing the AEs iteratively against all these models. We conduct experiments here to demonstrate that

SAM and *SAM&JR* can further enhance this ensemble and analyze how their intrinsic mechanisms correlate with LGV.

In Tab. IV, we fine-tune models well-trained with SGD³, *SAM*, and *SAM&JR* on CIFAR-10 with a constant learning rate of 0.05. The results show that LGV with *SAM*, *SAM&JR* can always yield superior ASRs than standard SGD, indicating that the underlying property of *SAM* and *JR* allows them to find solutions that benefit transferability. More intriguingly, fine-tuning models obtained by *SAM* and *SAM&JR* with standard SGD always brings non-negligible negative impacts on transferability. These suggest solutions well-trained with *SAM* and *SAM&JR* lie in the *basin of attractions* featuring better transferability. Besides, a relatively high constant learning rate with SGD will arbitrarily minimize the training loss while leaving the basin of attractions, and matters in obtaining a large vicinity, as stressed in [21]. Furthermore, we can infer that a large vicinity is unlikely to be a determining factor for transferability, since a single surrogate may outperform an ensemble of poor surrogates (see *SAM&JR* and *ST+LGV_{SGD}*). Instead, a dense subspace whose geometry is intrinsically connected to transferability is more desirable.

Incorporating other strategies. We take AE generation and ensemble strategies, which are the most well-explored methods, to exemplify the universality of better surrogates. We are aware of other factors that could also contribute to transferability, such as loss object modification [28, 70], architecture selection [61], and l_2 -norm consideration [36]. We leave it to our future work to investigate whether they can be mildly integrated with our design.

VI. ANALYSES AND DISCUSSIONS

Q1: Does the trade-off between smoothness and similarity really “predominate” transferability w.r.t. surrogates? Our theoretical analysis and experimental validation have demonstrated the significant role of smoothness and similarity in determining transferability among surrogate-side factors. However, it may still be uncertain whether they are more important factors than others (*i.e.*, accuracy and fooling probability), as claimed in Section II-C. To address this, we use Pearson correlation coefficients between these factors and ASR and run ordinary least squares (OLS) regressions to measure their joint effect on ASR. Tab. V reports the results under each fixed target model and adversarial budget, which indicates that both smoothness and similarity are highly correlated to ASR, with a clear superiority over other factors. Besides, the joint effect of smoothness and similarity (R_1^2) is significant in each case and very close to that of the 4 factors combined (R_2^2). Further, it does not exhibit a strong correlation with ϵ under each target model. These imply that the joint effect of smoothness and similarity is strong and robust, see Fig. 12 in the Appendix.

Interestingly, we can observe that as ϵ increases, the relevance w.r.t. smoothness alone increases, and the relevance w.r.t. similarity alone decreases. This agrees with the intuition:

³We refer SGD here to training models without any auxiliary augmentation or regularization mechanisms, not merely the particular optimizer itself.

TABLE V: The Pearson correlation coefficients (r) between ASR and accuracy (Acc), fooling probability (FP), model smoothness (MS), and gradient similarity (GS). For the coefficient of determination (R^2) in OLS, R_1^2 depicts the joint effect of MS and GS on ASR and R_2^2 depicts the joint effect of these 4 factors.

	CIFAR-10			
	ResNet50	VGG16	InceptionV3	DenseNet121
	$\frac{4}{755}$	$\frac{8}{755}$	$\frac{16}{755}$	$\frac{4}{755}$
$r(Acc, ASR)$	0.121 -0.049 -0.255	0.032 -0.095 -0.259	0.211 0.028 -0.187	0.286 0.130 -0.107
$r(FP, ASR)$	0.118 0.106 0.055	0.197 0.164 0.098	0.105 0.091 0.040	0.051 0.008 -0.033
$r(MS, ASR)$	0.540 0.662 0.753	0.614 0.700 0.774	0.478 0.630 0.732	0.418 0.581 0.701
$r(GS, ASR)$	0.912 0.837 0.759	0.924 0.878 0.816	0.864 0.743 0.653	0.875 0.710 0.585
R_1^2	0.909 0.885 0.879	0.917 0.906 0.893	0.870 0.827 0.838	0.880 0.773 0.765
R_2^2	0.943 0.892 0.894	0.931 0.907 0.913	0.911 0.843 0.852	0.926 0.823 0.799

	ImageNet			
	VGG16	DenseNet121	MobileNetV2	Xception
	$\frac{4}{755}$	$\frac{8}{755}$	$\frac{16}{755}$	$\frac{4}{755}$
$r(Acc, ASR)$	0.218 0.128 -0.047	0.133 0.023 -0.165	0.093 -0.014 -0.196	0.072 -0.028 -0.177
$r(FP, ASR)$	0.121 0.120 -0.055	0.146 0.117 -0.081	-0.034 0.003 -0.151	0.062 -0.012 -0.156
$r(MS, ASR)$	0.410 0.472 0.516	0.458 0.503 0.492	0.495 0.576 0.625	0.499 0.571 0.624
$r(GS, ASR)$	0.864 0.829 0.764	0.859 0.855 0.853	0.789 0.766 0.780	0.753 0.722 0.721
R_1^2	0.854 0.841 0.780	0.821 0.843 0.832	0.715 0.742 0.804	0.688 0.704 0.752
R_2^2	0.871 0.847 0.798	0.854 0.850 0.867	0.750 0.752 0.833	0.712 0.707 0.781

smoothness depicts the gradient invariance around original samples, while similarity captures the alignment of two gradients in different directions. As ϵ approaches 0, smoothness becomes less important for the gradient may not vary too much in a small region, and the right direction becomes more crucial since there is limited scope for success. As ϵ gets bigger, the alignment at the origin requires better smoothness to be further propagated into a bigger region. These suggest an adaptive similarity-smoothness trade-off surrogate could be preferable given different ϵ .

Q2: What if the target model is not trained on \mathcal{D} ? So far, we presume the target models are trained within the normal data distribution \mathcal{D} to lay out our analysis and conclusions, which is also set by default in Demontis *et al.* [9]. To verify the generality of the obtained conclusion, we deliver the results here when the data distribution restrictions of the target model \mathcal{G} is relaxed. First, we generalize Hypothesis 1 as:

Hypothesis 2 (\mathcal{D} -surrogate align general target models better than \mathcal{D}' -surrogate). Suppose surrogate models $\mathcal{F}_{\mathcal{D}}$ and $\mathcal{F}_{\mathcal{D}'}$ are trained on \mathcal{D} and \mathcal{D}' , respectively. Denote the data distribution of target model $\mathcal{G}_{\mathcal{D}_t}$ as $\mathcal{D}_t \in \mathcal{P}_{\mathcal{X} \times \mathcal{Y}}$. They all share a joint training loss ℓ . Then $\mathbb{E}_{\mathcal{D}_t \sim P_{\mathcal{X} \times \mathcal{Y}}} [\mathcal{S}_{\mathcal{D}}(\ell_{\mathcal{F}_{\mathcal{D}}}, \ell_{\mathcal{G}_{\mathcal{D}_t}}) - \mathcal{S}(\ell_{\mathcal{F}_{\mathcal{D}}}, \ell_{\mathcal{G}_{\mathcal{D}_t}})] < 0$ generally holds.

This hypothesis considers a more practical case that the adversary has no knowledge of \mathcal{D}_t , and tries to attack $\mathcal{G}_{\mathcal{D}_t}$ with AEs constructed on normal samples $(x, y) \in \mathcal{D}$. The adversary hopes its surrogate aligns well with any $\mathcal{G}_{\mathcal{D}_t}$ regardless of \mathcal{D}_t . We show that \mathcal{D} -surrogate $\mathcal{F}_{\mathcal{D}}$ is still better than \mathcal{D}' -surrogate $\mathcal{F}'_{\mathcal{D}}$ based on the expectation of various \mathcal{D}_t .

Tab. VI reports the general surrogate-target gradient similarities. It's obvious that \mathcal{D}' surrogates (above AT) generally worsen the gradient alignments as their increment scores are all negative, except for AT with a small budget $\epsilon = 0.01$. Conversely, the scores of \mathcal{D} surrogates (below AT) are all non-negative and most of them improve the general alignment. Note that when \mathcal{D}' happens to be \mathcal{D}_t , the gradient similarity

TABLE VI: **Cross-architecture** gradient similarity between surrogate-target pairs (ResNet18-VGG16) on CIFAR-10. The first row reports the results of *ST* surrogate, below which report the difference to *ST*. The last column rates the score of the surrogates based on the general alignment toward multiple targets. (Accumulate +1 for positive, -1 for negative values.)

Surrogate \ Target	<i>ST</i>	<i>CO</i>	<i>CM</i>	<i>MU</i>	<i>LS</i>	<i>AT</i> $\epsilon = 0.01$	Increment Score
<i>ST</i>	0.141	0.135	0.056	0.038	0.014	0.131	0
<i>CO</i>	-0.038	+0.005	-0.001	+0.004	-0.001	-0.041	-2
<i>CM</i>	-0.105	-0.084	+0.008	-0.021	-0.006	-0.098	-4
<i>MU</i>	-0.106	-0.092	-0.030	+0.122	-0.003	-0.102	-4
<i>LS</i>	-0.094	-0.098	-0.033	-0.013	+0.008	-0.090	-4
<i>AT</i> , $\epsilon = 0.01$	-0.002	-0.005	-0.013	+0.001	+0.001	+0.047	0
<i>IR</i>	-0.002	-0.014	-0.020	+0.008	+0.007	+0.043	0
<i>JR</i>	+0.044	+0.028	+0.004	+0.012	+0.004	+0.072	+6
<i>ER</i>	+0.012	+0.006	-0.013	+0.011	+0.005	+0.031	+4
<i>SAM</i>	+0.055	+0.057	+0.007	+0.029	+0.006	+0.058	+6
<i>SAM&IR</i>	+0.012	+0.001	-0.021	+0.016	+0.010	+0.065	+4
<i>SAM&JR</i>	+0.078	+0.072	+0.008	+0.035	+0.010	+0.093	+6

between $\mathcal{F}'_{\mathcal{D}}$ and $\mathcal{G}_{\mathcal{D}_t}$ is high, especially for *CM* and *MU*. However, these surrogates lower the similarity towards all other targets. In general, they are not good surrogates since \mathcal{D}_t is unknown to the adversary.

The same observations apply to the transfer ASRs. Tab. X reports the transfer ASRs against various $\mathcal{G}_{\mathcal{D}_t}$ that are not trained on \mathcal{D} . Even when surrogates have the same training mechanisms as the corresponding target models, the best surrogate is still either *SAM&IR* or *SAM&JR*, regardless of what \mathcal{D}_t is. This finding is in line with the results in Tab. II.

Q3: What is the relationship between model smoothness and model complexity? Model complexity has been investigated in Demontis *et al.* [9] to figure out whether it correlates with transferability, which is defined as the variability of the loss landscape, deriving from the number of local optima of the surrogates. Here we correlate the number of local optima with model smoothness. It is obvious that a high-complexity model featuring multiple local optima will cause a larger variance to the loss landscape of adversarial example optimization. Formally, for a feature x , the fewer optima in its ϵ -neighbor, the smaller the variance would be. Thus, supposing the loss function used to optimize adversarial points is continuously differentiable, by promoting the smoothness, we can expect fewer optima in the finite ϵ -neighbor space since all the local optima are wider. Consequently, model smoothness negatively correlates with model complexity, *i.e.*, a smoother model indicates lower complexity.

Q4: Does a smaller model generalization gap imply higher adversarial transferability? It is natural to raise this question as the idea of adversarial transferability in a way resembles the concept of model generalization. The former captures the effectiveness of AEs against unseen models, while the latter evaluates the model’s ability to adapt properly to previously unseen data. A concurrent work [58] attempts to show the positive relationship between model generalization and adversarial transferability, by applying a spectral normalization method constraining the L_2 -operator norm of the surrogate’s

TABLE VII: Untargeted transfer ASRs of AEs crafted against ViT ImageNet surrogates on target models. In %.

Source	Acc	Normally Trained					Adversarially Trained	
		Res101	Dense121	VGG16	IncV3	IncV3 _{AT}	IncResV3 _{AT}	
ViT-B/16	84.5	23.8	37.6	50.0	45.9	48.6	27.6	
ViT-B/16-SAM	80.2	48.4	69.9	75.2	70.2	59.5	40.5	
ViT-B/32	80.7	19.6	35.7	50.0	49.1	51.9	29.7	
ViT-B/32-SAM	73.7	34.0	55.8	68.9	64.3	63.1	43.9	
ViT-B/16+DIM	84.5	60.7	75.3	79.9	80.0	61.4	43.8	
ViT-B/16-SAM+DIM	80.2	81.6	95.6	93.9	94.6	82.4	79.9	
ViT-B/32+DIM	80.7	48.4	66.4	75.2	81.6	68.6	54.4	
ViT-B/32-SAM+DIM	73.7	48.9	78.1	78.4	82.5	79.3	72.3	

weight matrix to empirically demonstrate the increase of both transferability and generalization.

Nevertheless, we emphasize that we cannot over-generalize the alignment between generalization and transferability. It is easy to find some methods that boost generalization while degrading transferability (*e.g.*, through damaging similarity). For example, the results in Tabs. II, VIII, XII and XIII have shown that changing data distribution to boost generalization could sacrifice transferability. More typically, the strong data augmentations that yield the smallest generalization gaps (see Tab. XI) perform the worst in transfer attacks. In fact, the product of spectral norm (L_2 -norm) of the model’s layer-wise weight matrices is a loose upper bound of $\|\nabla_x f_\theta(x)\|_2$ [46, 66]. When $\|\nabla_x f_\theta(x)\|_2 \rightarrow 0$, we have $\|\nabla_x f_\theta(x)\|_F \rightarrow 0$. Utilizing Proposition 1, we also have $\|\nabla_x \ell(f_\theta(x), y)\| \rightarrow 0$. This suggests that spectral normalization actually benefits transferability by promoting smoothness.

Q5: What is restraining the adversarial transferability of ViT? Recently, ViT [14] receives notable attention for its outstanding performance on various tasks. Meanwhile, some works [35, 47] have demonstrated that ViT models exhibit lower adversarial transferability than CNNs when used as surrogates, and a recent work [41] argues that this is because the current attacks are not strong enough to fully exploit the transferability potential of ViT. Complementarily, we provide a different viewpoint that *the transferability of ViT may have been restrained by its own training paradigm*. ViT is known to have poor trainability [6, 7, 56], and thus generally requires large-scale pre-training and fine-tuning with strong data augmentations. This training paradigm is used by default since its appearance. However, as we discussed in this paper, changing the data distribution could have negative impacts on similarity. Using data augmentation is plausible for accuracy performance, yet not ideal for transfer attacks.

To validate this standpoint, we show that with a different training method, such as using *SAM*, the transferability of ViT can be significantly improved. Our experiments are conducted on well-trained ImageNet classifiers, all publicly available from PyTorch image model library timm [60]. We consider standard ViT surrogates ViT-B/16 and ViT-B/32, which are both first pre-trained on a large-scale dataset and then fine-tuned on ImageNet using a combination of *MU* and RandAugment [8]. In contrast, their *SAM* versions ViT-B/16-SAM and ViT-B/32-SAM are trained from scratch. We use both normally trained and adversarially trained CNN classifiers

TABLE VIII: Transfer ASRs under the different L_∞ budgets on 3 MLaaS platforms using AEs reported in Tab. XIII.

Model	Untargeted			Targeted		
	AWS 8 255	Baidu 16 255	Aliyun 8 255	AWS 8 255	Baidu 16 255	Aliyun 8 255
ST	9.4	13.4	30.0	53.8	18.6	52.2
MU	8.6	10.8	20.4	39.6	12.4	33.8
CM	8.0	10.8	19.4	35.0	12.4	29.2
CO	9.6	13.0	27.2	48.4	18.6	51.8
LS	9.6	12.0	23.4	43.0	12.2	33.6
AT, $\epsilon = 1$	9.6	24.0	38.2	60.4	35.0	82.6
AT, $\epsilon = 5$	7.8	16.0	22.2	53.4	15.6	60.0
IR	10.4	23.6	45.8	60.0	48.8	86.0
JR	9.8	22.6	46.4	60.6	48.2	79.6
ER	9.8	13.4	28.2	56.2	24.0	56.6
SAM	10.2	16.4	37.2	59.2	36.2	68.2
SAM&IR	11.0	28.4	54.2	63.8	55.8	93.4
SAM&JR	11.4	16.2	45.8	61.2	48.0	79.0

as target models. We craft AEs on these 4 surrogates using both standard PGD and DIM strategies under $\epsilon = 16/255$ on the popular ImageNet-compatible dataset as in [44]. The accuracy of these surrogates (referring to [60]) and the ASRs are reported in Tab. VII. The results indicate that standard ViT models have much weaker transferability than their SAM versions, despite the fact that they have higher accuracy.

Q6: Will the transferability benefit of better surrogate in “lab” generalize to “real-world” environment? Recently, Mao *et al.* [36] suggests that many conclusions about adversarial transferability done in the simplistic controlled “lab” environments may not hold in the real world. We thus conduct experiments here to verify the generality of our conclusions using the AEs crafted against our local ImageNette surrogates.

Specifically, aligning with Mao *et al.* [36], we conduct transfer attacks on three commercial MLaaS platforms—AWS Rekognition, Alibaba Cloud, and Baidu Cloud, using their code, and report the results in Tab. VIII. The experimental settings can be found in the Appendix. The results are generally consistent with that in Tab. XIII. Particularly, we highlight here that our experimental results on MLaaS platforms **contradict** the observation in Mao *et al.* [36] that “adversarial training and data augmentation do not show strong correlations to the transfer attack”. Tab. VIII indicates that strong data augmentations like CM and MU generally exhibit lower ASRs than ST for both targeted and untargeted attacks. In addition, we can observe that “little robustness” (see AT, $\epsilon = 1$) improves transferability while large adversarial magnitude (see AT, $\epsilon = 5$) degrades it.

Q7: How does SAM yield superior alignment towards every training solution? Given its superior performance on transferability and gradient alignment, it is natural to wonder why SAM exhibits this property. Recent work [29] empirically demonstrates that attacking an ensemble of models in the distribution obtained via *Bayesian* learning substantially improves the transferability. Another concurrent work [39] theoretically establishes SAM as an optimal relaxation of Bayes object. Consequently, this suggests that the transferability advantage of SAM may be attributed to the fact it optimizes a single model that represents an ensemble (expectation) of various models in some way, *i.e.*, attacking a SAM solution is equivalent to attacking an ensemble of solutions. We further conjecture that

the strong input gradient alignment towards every training solution may reflect this high-level “expectation” effect of SAM (Bayes). Notably, our interpretation here is merely intuitive and speculative, and SAM remains poorly understood to date, with its generalization benefit not yet entirely understood. We believe that uncovering the exact reason is far beyond the scope of our paper, while our experimental observations provide valuable insights and may contribute to a better understanding of SAM for future studies.

VII. RELATED WORK

Our aim is to provide a comprehensive overview of adversarial transferability from the surrogate training perspective. We examine how model smoothness and gradient similarity are affected under various training mechanisms. Our goal is ultimately to find an approach that optimizes these two factors simultaneously during surrogate training.

Intriguingly, we note that some concurrent works adopt similar design philosophies from other perspectives of adversarial transferability. Wu *et al.* [62] propose a regularization term that encourages small loss gradient norms in the input space when finding local optima during adversarial example generation. Ge *et al.* [18] also propose a similar regularization term for penalizing the gradient norm along with gradient averaging on multiple randomly sampled neighbors. On the other hand, Chen *et al.* [5] study the model ensemble perspective and propose a common weakness attack. They adopt sharpness-aware minimization and a cosine similarity encourager to converge the adversarial example to a point close to a flat local optimum of each model. To summarize, these works also have demonstrated the effectiveness of optimizing model smoothness and gradient similarity for improving adversarial transferability. Our work complements theirs by viewing transferability as an inherent property of the surrogate model itself. We propose methods to construct surrogate models specialized for transfer attacks by optimizing smoothness and similarity.

VIII. CONCLUSION

In this paper, we have conducted a comprehensive analysis of the transferability of adversarial examples from the surrogate perspective. To the best of our knowledge, this is the first in-depth study on obtaining better surrogates for transfer attacks. We have proposed and examined two working hypotheses. The first one is that the trade-off between model smoothness and gradient similarity largely dictates adversarial transferability from the perspective of surrogate models. The other one is that the data distribution shift will impair gradient similarity, thereby producing worse surrogates on average. The practical guide for more effective transfer attacks is to handle these model smoothness and similarity well simultaneously, validated by our proposed methods, *i.e.*, the combination of input gradient regularization and sharpness-aware minimization. On the other front, our study also exemplifies the conflicting aspects of current research and further provides plausible explanations for some intriguing puzzles while revealing other unsolved issues in the study of adversarial transferability.

REFERENCES

- [1] Momin Abbas, Quan Xiao, Lisha Chen, Pin-Yu Chen, and Tianyi Chen. Sharp-MAML: Sharpness-Aware Model-Agnostic Meta Learning. In *Proc. of the 39th International Conference on Machine Learning (ICML)*, pages 10–32, 2022.
- [2] Maksym Andriushchenko and Nicolas Flammarion. Towards Understanding Sharpness-Aware Minimization. In *Proc. of the 39th International Conference on Machine Learning (ICML)*, pages 639–668, 2022.
- [3] David Barrett and Benoit Dherin. Implicit Gradient Regularization. In *International Conference on Learning Representations*, 2021.
- [4] Alvin Chan, Yi Tay, Yew Soon Ong, and Jie Fu. Jacobian Adversarially Regularized Networks for Robustness. In *Proc. of the 8th International Conference on Learning Representations (ICLR)*, 2020.
- [5] Huanran Chen, Yichi Zhang, Yinpeng Dong, and Jun Zhu. Rethinking model ensemble in transfer-based adversarial attacks. *arXiv preprint arXiv:2303.09105*, 2023.
- [6] Xiangning Chen, Cho-Jui Hsieh, and Boqing Gong. When Vision Transformers Outperform ResNets without Pre-training or Strong Data Augmentations. In *Proc. of the 10th International Conference on Learning Representations (ICLR)*, 2022.
- [7] Xinlei Chen, Saining Xie, and Kaiming He. An Empirical Study of Training Self-Supervised Vision Transformers. In *Proc. of IEEE/CVF International Conference on Computer Vision (ICCV)*, pages 9640–9649, 2021.
- [8] Ekin D. Cubuk, Barret Zoph, Jonathon Shlens, and Quoc V. Le. Randaugment: Practical Automated Data Augmentation With a Reduced Search Space. In *Proc. of the IEEE/CVF Conference on Computer Vision and Pattern Recognition (CVPR) Workshops*, pages 702–703, 2020.
- [9] Ambra Demontis, Marco Melis, Maura Pintor, Matthew Jagielski, Battista Biggio, Alina Oprea, Cristina Nita-Rotaru, and Fabio Roli. Why Do Adversarial Attacks Transfer? Explaining Transferability of Evasion and Poisoning Attacks. In *Proc. of the 28th USENIX Security Symposium (USENIX Security)*, 2019.
- [10] Terrance DeVries and Graham W Taylor. Improved Regularization of Convolutional Neural Networks with Cutout. *arXiv preprint arXiv:1708.04552*, 2017.
- [11] Benoit Dherin, Michael Munn, Mihaela Rosca, and David Barrett. Why Neural Networks Find Simple Solutions: the Many Regularizers of Geometric Complexity. *Advances in Neural Information Processing Systems*, 35:2333–2349, 2022.
- [12] Yinpeng Dong, Fangzhou Liao, Tianyu Pang, Hang Su, Jun Zhu, Xiaolin Hu, and Jianguo Li. Boosting Adversarial Attacks with Momentum. In *Proc. of the 2018 IEEE Conference on Computer Vision and Pattern Recognition (CVPR)*, pages 9185–9193, 2018.
- [13] Yinpeng Dong, Tianyu Pang, Hang Su, and Jun Zhu. Evading Defenses to Transferable Adversarial Examples by Translation-Invariant Attacks. In *Proceedings of the IEEE/CVF Conference on Computer Vision and Pattern Recognition (CVPR)*, 2019.
- [14] Alexey Dosovitskiy, Lucas Beyer, Alexander Kolesnikov, Dirk Weissenborn, Xiaohua Zhai, Thomas Unterthiner, Mostafa Dehghani, Matthias Minderer, Georg Heigold, Sylvain Gelly, Jakob Uszkoreit, and Neil Houlsby. An Image is Worth 16x16 Words: Transformers for Image Recognition at Scale. In *Proc. of the 9th International Conference on Learning Representations (ICLR)*, 2021.
- [15] Harris Drucker and Yann Le Cun. Improving Generalization Performance Using Double Backpropagation. *IEEE Transactions on Neural Networks*, 3(6):991–997, 1992.
- [16] Jiawei Du, Hanshu Yan, Jiashi Feng, Joey Tianyi Zhou, Liangli Zhen, Rick Siow Mong Goh, and Vincent Tan. Efficient Sharpness-aware Minimization for Improved Training of Neural Networks. In *Proc. of the 10th International Conference on Learning Representations (ICLR)*, 2022.
- [17] Pierre Foret, Ariel Kleiner, Hossein Mobahi, and Behnam Neyshabur. Sharpness-aware Minimization for Efficiently Improving Generalization. In *Proc. of the 9th International Conference on Learning Representations (ICLR)*, 2021.
- [18] Zhijin Ge, Fanhua Shang, Hongying Liu, Yuanyuan Liu, and Xiaosen Wang. Boosting adversarial transferability by achieving flat local maxima. *arXiv preprint arXiv:2306.05225*, 2023.
- [19] Jonas Geiping, Micah Goldblum, Phil Pope, Michael Moeller, and Tom Goldstein. Stochastic Training is Not Necessary for Generalization. In *International Conference on Learning Representations (ICLR)*, 2022.
- [20] Justin Gilmer, Luke Metz, Fartash Faghri, Samuel S. Schoenholz, Maithra Raghu, Martin Wattenberg, and Ian J. Goodfellow. Adversarial Spheres. In *Proc. of the 6th International Conference on Learning Representations (ICLR) Workshop*, 2018.
- [21] Martin Gubri, Maxime Cordy, Mike Papadakis, Yves Le Traon, and Koushik Sen. LGV: Boosting Adversarial Example Transferability from Large Geometric Vicinity. In *Proc. of the European Conference on Computer Vision (ECCV)*, pages 603–618, 2022.
- [22] Yiwen Guo, Qizhang Li, and Hao Chen. Backpropagating Linearly Improves Transferability of Adversarial Examples. In *Advances in Neural Information Processing Systems (NeurIPS)*, volume 33, pages 85–95, 2020.
- [23] Judy Hoffman, Daniel A. Roberts, and Sho Yaida. Robust Learning with Jacobian Regularization. *arXiv preprint arXiv:1908.02729*, 2019.
- [24] Daniel Jakubovitz and Raja Giryes. Improving DNN Robustness to Adversarial Attacks using Jacobian Regularization. In *Proc. of the European Conference on Computer Vision (ECCV)*, pages 514–529, 2018.
- [25] Ryo Karakida, Tomoumi Takase, Tomohiro Hayase, and Kazuki Osawa. Understanding Gradient Regularization in Deep Learning: Efficient Finite-Difference Computation and Implicit Bias. *arXiv preprint arXiv:2210.02720*, 2022.
- [26] Marc Khouri and Dylan Hadfield-Menell. On the Geometry of Adversarial Examples, 2019.
- [27] Junhyung Kwon and Sangkyun Lee. Improving the Robustness of Model Compression by On-Manifold Adversarial Training. *Future Internet*, 13(12):300, 2021.
- [28] Maosen Li, Cheng Deng, Tengjiao Li, Junchi Yan, Xinbo Gao, and Heng Huang. Towards Transferable Targeted Attack. In *Proceedings of the IEEE/CVF Conference on Computer Vision and Pattern Recognition (CVPR)*, 2020.
- [29] Qizhang Li, Yiwen Guo, Wangmeng Zuo, and Hao Chen. Making Substitute Models More Bayesian Can Enhance Transferability of Adversarial Examples. In *Proc. of the 11th International Conference on Learning Representations (ICLR)*, 2023.
- [30] Wei-An Lin, Chun Pong Lau, Alexander Levine, Rama Chellappa, and Soheil Feizi. Dual Manifold Adversarial Robustness: Defense against Lp and non-Lp Adversarial Attacks. *Advances in Neural Information Processing Systems*, 33:3487–3498, 2020.
- [31] Yanpei Liu, Xinyun Chen, Chang Liu, and Dawn Song. Delving into Transferable Adversarial Examples and Black-box Attacks. In *Proc. of the 5th International Conference on Learning Representations (ICLR)*, 2017.
- [32] Yong Liu, Siqi Mai, Xiangning Chen, Cho-Jui Hsieh, and Yang You. Towards Efficient and Scalable Sharpness-Aware Minimization. In *Proc. of the IEEE/CVF Conference on Computer Vision and Pattern Recognition (CVPR)*, pages 12360–12370, 2022.
- [33] Xingjun Ma, Bo Li, Yisen Wang, Sarah M. Erfani, Sudanthi Wijewickrema, Grant Schoenebeck, Michael E. Houle, Dawn Song, and James Bailey. Characterizing Adversarial Subspaces Using Local Intrinsic Dimensionality. In *Proc. of the 6th International Conference on Learning Representations (ICLR)*, 2018.
- [34] Aleksander Madry, Aleksandar Makelov, Ludwig Schmidt, Dimitris Tsipras, and Adrian Vladu. Towards Deep Learning Models Resistant to Adversarial Attacks. In *Proc. of the International Conference on Learning Representations (ICLR)*, 2018.
- [35] Kaleel Mahmood, Rigel Mahmood, and Marten van Dijk. On the robustness of vision transformers to adversarial examples. In *Proc. of IEEE/CVF International Conference on Computer Vision (ICCV)*, pages 7838–7847, 2021.
- [36] Yuhao Mao, Chong Fu, Saizhuo Wang, Shouling Ji, Xuhong Zhang, Zhenguang Liu, Jun Zhou, Alex Liu, Raheem Beyah, and Ting Wang. Transfer Attacks Revisited: A Large-Scale Empirical Study in Real Computer Vision Settings. In *IEEE*

Symposium on Security and Privacy (SP), pages 1423–1439, 2022.

[37] James Martens, Ilya Sutskever, and Kevin Swersky. Estimating the Hessian by Back-propagating Curvature. In *Proc. of the 29th International Conference on Machine Learning (ICML)*, pages 963–970, 2012.

[38] Peng Mi, Li Shen, Tianhe Ren, Yiyi Zhou, Xiaoshuai Sun, Rongrong Ji, and Dacheng Tao. Make Sharpness-Aware Minimization Stronger: A Sparsified Perturbation Approach. In *Advances in Neural Information Processing Systems*, 2022.

[39] Thomas Möllenhoff and Mohammad Emtiyaz Khan. SAM as an Optimal Relaxation of Bayes. In *Proc. of the 11th International Conference on Learning Representations (ICLR)*, 2023.

[40] Muzammal Naseer, Salman Khan, Munawar Hayat, Fahad Shahbaz Khan, and Fatih Porikli. On Generating Transferable Targeted Perturbations. In *Proc. of the 2021 IEEE/CVF International Conference on Computer Vision (ICCV)*, pages 7708–7717, 2021.

[41] Muzammal Naseer, Kanchana Ranasinghe, Salman Khan, Fahad Khan, and Fatih Porikli. On Improving Adversarial Transferability of Vision Transformers. In *Proc. of the 10th International Conference on Learning Representations (ICLR)*, 2022.

[42] Adam Paszke, Sam Gross, Soumith Chintala, Gregory Chanan, Edward Yang, Zachary DeVito, Zeming Lin, Alban Desmaison, Luca Antiga, and Adam Lerer. Automatic Differentiation in PyTorch. 2017.

[43] Kainal Patel, William Beluch, Dan Zhang, Michael Pfeiffer, and Bin Yang. On-manifold Adversarial Data Augmentation Improves Uncertainty Calibration. In *Proc. of the 25th International Conference on Pattern Recognition (ICPR)*, pages 8029–8036, 2020.

[44] Zeyu Qin, Yanbo Fan, Yi Liu, Li Shen, Yong Zhang, Jue Wang, and Baoyuan Wu. Boosting the Transferability of Adversarial Attacks with Reverse Adversarial Perturbation. In *Advances in Neural Information Processing Systems (NeurIPS)*, 2022.

[45] Andrew Ross and Finale Doshi-Velez. Improving the adversarial robustness and interpretability of deep neural networks by regularizing their input gradients. In *Proc. of the AAAI Conference on Artificial Intelligence*, 2018.

[46] Kevin Roth, Yannic Kilcher, and Thomas Hofmann. Adversarial training is a form of data-dependent operator norm regularization. *Advances in Neural Information Processing Systems (NeurIPS)*, 33:14973–14985, 2020.

[47] Rulin Shao, Zhouxing Shi, Jinfeng Yi, Pin-Yu Chen, and Chou-jui Hsieh. On the Adversarial Robustness of Vision Transformers. In *Annual Conference on Neural Information Processing Systems*, 2022.

[48] Samuel L Smith, Benoit Dherin, David Barrett, and Soham De. On the Origin of Implicit Regularization in Stochastic Gradient Descent. In *Proc. of the 9th International Conference on Learning Representations (ICLR)*, 2021.

[49] Jure Sokolić, Raja Giryes, Guillermo Sapiro, and Miguel RD Rodrigues. Robust Large Margin Deep Neural Networks. *IEEE Transactions on Signal Processing*, 65(16):4265–4280, 2017.

[50] Yang Song, Taesup Kim, Sebastian Nowozin, Stefano Ermon, and Nate Kushman. PixelDefend: Leveraging Generative Models to Understand and Defend against Adversarial Examples. In *International Conference on Learning Representations (ICLR)*, 2018.

[51] Jacob Springer, Melanie Mitchell, and Garrett Kenyon. A Little Robustness Goes a Long Way: Leveraging Robust Features for Targeted Transfer Attacks. *Advances in Neural Information Processing Systems (NeurIPS)*, 34:9759–9773, 2021.

[52] Jacob M Springer, Melanie Mitchell, and Garrett T Kenyon. Uncovering Universal Features: How Adversarial Training Improves Adversarial Transferability. In *ICML 2021 Workshop on Adversarial Machine Learning*, 2021.

[53] David Stutz, Matthias Hein, and Bernt Schiele. Disentangling Adversarial Robustness and Generalization. In *Proceedings of the IEEE/CVF Conference on Computer Vision and Pattern Recognition (CVPR)*, June 2019.

[54] Christian Szegedy, Wojciech Zaremba, Ilya Sutskever, Joan Bruna, Dumitru Erhan, Ian Goodfellow, and Rob Fergus. Intriguing Properties of Neural Networks. *arXiv preprint arXiv:1312.6199*, 2013.

[55] Szegedy, Christian and Vanhoucke, Vincent and Ioffe, Sergey and Shlens, Jon and Wojna, Zbigniew. Rethinking the Inception Architecture for Computer Vision. In *Proc. of the IEEE conference on computer vision and pattern recognition*, pages 2818–2826, 2016.

[56] Hugo Touvron, Matthieu Cord, Matthijs Douze, Francisco Massa, Alexandre Sablayrolles, and Hervé Jegou. Training data-efficient image transformers: distillation through attention. In *Proc. of the 38th International Conference on Machine Learning (ICML)*, volume 139 of *Proceedings of Machine Learning Research*, pages 10347–10357, 2021.

[57] Dániel Varga, Adrián Csizsárík, and Zsolt Zombori. Gradient Regularization Improves Accuracy of Discriminative Models. *arXiv preprint arXiv:1712.09936*, 2017.

[58] Yilin Wang and Farzan Farnia. On the Role of Generalization in Transferability of Adversarial Examples. *arXiv preprint arXiv:2206.09238*, 2022.

[59] Kaiyue Wen, Tengyu Ma, and Zhiyuan Li. How Does Sharpness-Aware Minimization Minimize Sharpness? In *Proc. of the 11th International Conference on Learning Representations (ICLR)*, 2023.

[60] Ross Wightman. PyTorch Image Models. <https://github.com/rwightman/pytorch-image-models>, 2019.

[61] Dongxian Wu, Yisen Wang, Shu-Tao Xia, James Bailey, and Xingjun Ma. Skip Connections Matter: On the Transferability of Adversarial Examples Generated with ResNets. In *International Conference on Learning Representations (ICLR)*, 2020.

[62] Tao Wu, Tie Luo, and Donald C Wunsch. Gnp attack: Transferable adversarial examples via gradient norm penalty. *arXiv preprint arXiv:2307.04099*, 2023.

[63] Jiancong Xiao, Liusha Yang, Yanbo Fan, Jue Wang, and Zhi-Quan Luo. Understanding Adversarial Robustness Against On-manifold Adversarial Examples. *arXiv preprint arXiv:2210.00430*, 2022.

[64] Cihang Xie, Zhishuai Zhang, Yuyin Zhou, Song Bai, Jianyu Wang, Zhou Ren, and Alan L Yuille. Improving Transferability of Adversarial Examples with Input Diversity. In *Proc. of the IEEE/CVF Conference on Computer Vision and Pattern Recognition*, pages 2730–2739, 2019.

[65] Zhuolin Yang, Linyi Li, Xiaojun Xu, Shiliang Zuo, Qian Chen, Pan Zhou, Benjamin Rubinstein, Ce Zhang, and Bo Li. TRS: Transferability Reduced Ensemble via Promoting Gradient Diversity and Model Smoothness. In *Advances in Neural Information Processing Systems (NeurIPS)*, pages 17642–17655, 2021.

[66] Yuichi Yoshida and Takeru Miyato. Spectral Norm Regularization for Improving the Generalizability of Deep Learning. *stat*, 1050:31, 2017.

[67] Sangdoo Yun, Dongyoon Han, Seong Joon Oh, Sanghyuk Chun, Junsuk Choe, and Youngjoon Yoo. CutMix: Regularization Strategy to Train Strong Classifiers with Localizable Features. In *Proc. of the IEEE/CVF international conference on computer vision*, pages 6023–6032, 2019.

[68] Hongyi Zhang, Moustapha Cisse, Yann N Dauphin, and David Lopez-Paz. Mixup: Beyond Empirical Risk Minimization. In *International Conference on Learning Representations (ICLR)*, 2018.

[69] Yang Zhao, Hao Zhang, and Xiuyuan Hu. Penalizing Gradient Norm for Efficiently Improving Generalization in Deep Learning. In *Proc. of the 39th International Conference on Machine Learning*, 2022.

[70] Zhengyu Zhao, Zhuoran Liu, and Martha Larson. On Success and Simplicity: A Second Look at Transferable Targeted Attacks. In *Advances in Neural Information Processing Systems (NeurIPS)*, pages 6115–6128, 2021.

[71] Qihuang Zhong, Liang Ding, Li Shen, Peng Mi, Juhua Liu, Bo Du, and Dacheng Tao. Improving Sharpness-Aware Minimization with Fisher Mask for Better Generalization on Language Models. *arXiv preprint arXiv:2210.05497*, 2022.

[72] Jun Tang Zhuang, Boqing Gong, Liangzhe Yuan, Yin Cui, Hartwig Adam, Nicha Dvornek, Sekhar Tatikonda, James Duncan, and Ting Liu. Surrogate gap minimization improves sharpness-aware training. In *International Conference on Learning Representations (ICLR)*, 2022.

APPENDIX

A. Experiments on ImageNette

Figs. 9 and 11 present the model smoothness in data augmentations and gradient regularization cases, and Fig. 10 plots gradient similarity towards different target models.

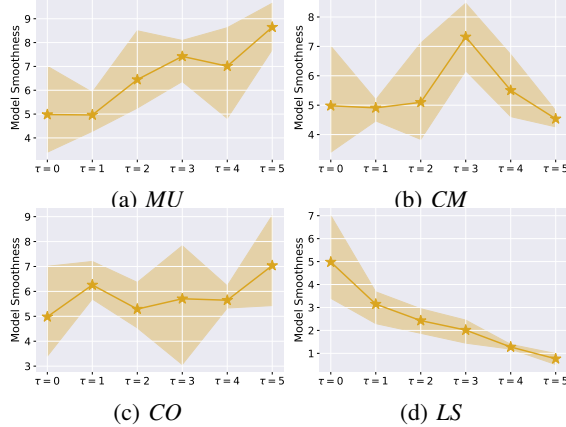


Figure 9: Smoothness of augmented ImageNette models.

B. Experimental Settings

Model training. We train the models from scratch on CIFAR-10 and finetune pre-trained ImageNet models on ImageNette. Please see Tab. IX for the detailed training settings.

Attacking MLaaS platforms. To conduct evaluations on MLaaS platforms, we follow the settings and metrics in [36] to design our experiments. Specifically, we choose ImageNette as the dataset and three leading commercial APIs as the victims, including AWS Rekognition, Aliyun (Alibaba Cloud), and Baidu Cloud. Since the MLaaS platforms return predictions with multiple labels, we first translate the local classes of ImageNette into lists $L_n = \sum_{i=1}^I \{y_{api} > \gamma_a \mid y_{api} \in API(x_i)\}$, where L_n represents the label list for the n -th class in ImageNette, x_i represents the samples in class n , and γ_a is the threshold. After constructing the label lists, we calculate the *attack success rate* (ASR) by:

$ASR = \frac{1}{I} \sum_{i=1}^I \mathcal{I}(API(x_i + \delta), L_n)$, where \mathcal{I} is an indicator function. For untargeted attacks, if a label exists both in the label list L_n and the API's prediction, meanwhile the confidence of this label is above a threshold γ_b , \mathcal{I} will return 0, which means the un-targeted attack has failed. Else \mathcal{I} will return 1; For targeted attacks, if a label exists both in the target label list L_{n+1} and the API's prediction, meanwhile the confidence of this label are above a threshold γ_b , \mathcal{I} will return 1, else \mathcal{I} will return 0. For AWS Rekognition, we set $\gamma_a = 99.99$ and $\gamma_b = 50.0$. For Aliyun, we set $\gamma_a = 50$ and $\gamma_b = 10$. And for Baidu Cloud, we set $\gamma_a = 0.5$ and $\gamma_b = 0.1$.

C. Proof of Transferability Lower Bound

Here we present the proof of Theorem 1. The following two lemmas are used in the proof.

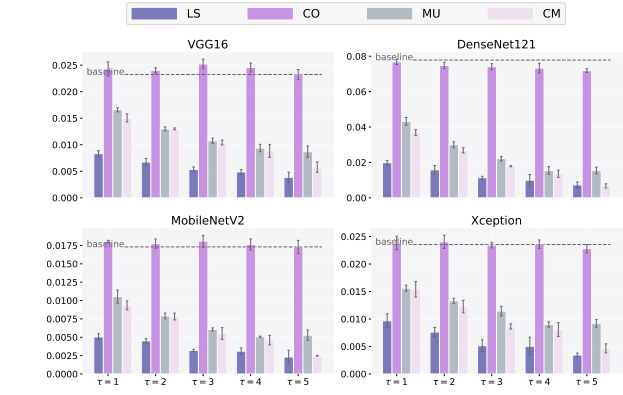


Figure 10: Gradient similarities between augmented ImageNette surrogates and ST target models.

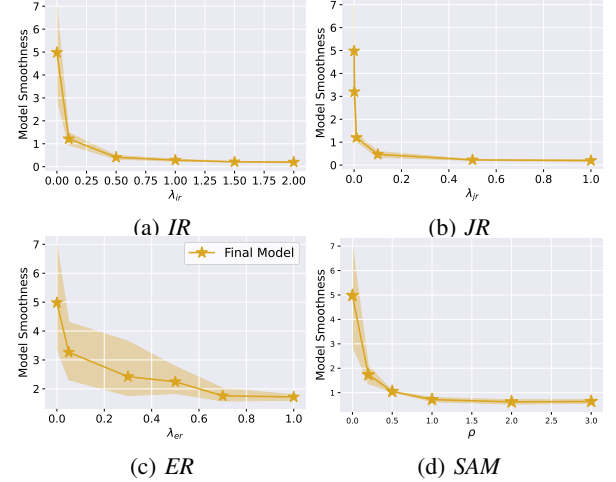


Figure 11: Model smoothness of regularized models (ResNet50) on ImageNette.

TABLE IX: Hyperparameters for training on CIFAR-10 and ImageNette. *MU*, *CM*, *CO* and *LS* refer to the X-axis parameters of Figs. 5, 6, 9 and 10. *AT* refer to Figs. 2 to 4. *IR*, *JR*, *ER* and *SAM* refer to Figs. 7 and 11, respectively. The bold items in parameter lists correspond to Tabs. II and XIII.

	CIFAR-10	ImageNette
Surrogate Architecture	ResNet18	ResNet50
Input size	32 × 32	224 × 224
Batch size	128	128
Epoch	200	50
Warmup epoch	10	5
Finetune	False	True
Peak learning rate	0.1	1
Learning rate decay	cosine	
Optimizer	SGD	
(<i>MU</i>) p	{0.1, 0.3, 0.5, 0.7, 0.9 }	
(<i>CM</i>) p	{0.1, 0.3, 0.5, 0.7, 0.9 }	
(<i>CO</i>) M	{8, 12, 16, 20, 24 }	{80, 100, 120, 140, 160 }
(<i>LS</i>) p	{0.1, 0.2, 0.3, 0.4, 0.5 }	
(<i>AT</i>) Step	10	5
(<i>AT</i>) Step_size	$0.25 \times \epsilon$	$0.4 \times \epsilon$
(<i>AT</i>) ϵ	{0.01, 0.03 , 0.05, 0.1, 0.2, 0.5, 1}	{0.05, 0.1, 0.2, 0.5, 1 , 3, 5}
(<i>IR</i>) λ_{ir}	{0.1, 0.3, 0.5 , 0.7, 1}	{0.1, 0.5, 1 , 1.5, 2}
(<i>JR</i>) λ_{jr}	{1e-5, 1e-4 , 0.01, 0.05, 0.1}	{0.001, 0.01, 0.1 , 0.5, 1}
(<i>ER</i>) λ_{er}	{1e-3, 5e-3, 0.01, 0.05 , 0.1}	{ 0.05 , 0.3, 0.5, 0.7, 1}
(<i>SAM</i>) ρ	{0.01, 0.05, 0.1 , 0.15, 0.2}	{ 0.2 , 0.5, 1, 2, 3}

Lemma 1. For arbitrary vector δ, x, y , suppose $\|\delta\|_2 \leq \epsilon, x$

TABLE X: Transfer ASRs of AEs crafted from various ResNet18 surrogates against VGG16 target models trained with *AT* and augmentations on CIFAR-10. \star denotes surrogates have the same training methods as the corresponding target models. ‘T’ represents ‘Targeted’ and ‘U’ represents ‘Untargeted’.

	$AT, \epsilon = 0.01$		$AT, \epsilon = 0.05$		CM		CO		LS		MU	
	T	U	T	U	T	U	T	U	T	U	T	U
<i>ST</i>	20.18	51.33	4.83	22.49	42.42	79.49	38.80	76.33	34.62	72.34	37.46	69.25
\star	43.01	76.96	35.54	69.56	14.20	54.57	32.91	79.11	11.90	46.66	15.81	54.43
<i>IR</i>	60.08	91.23	31.84	73.98	59.80	91.82	60.78	92.14	63.20	93.52	60.79	90.06
<i>JR</i>	57.24	83.54	14.57	41.77	73.44	92.47	74.77	93.03	72.27	92.30	68.34	86.90
<i>ER</i>	32.61	77.14	9.55	40.41	41.94	86.92	43.04	87.39	44.51	87.77	42.12	82.66
<i>SAM</i>	40.35	79.31	8.41	35.05	75.34	96.59	67.72	94.84	62.68	93.57	65.37	90.43
<i>SAM&JR</i>	71.88	94.01	48.38	80.88	70.81	93.75	73.05	94.31	74.02	95.47	70.81	92.68
<i>SAM&JR</i>	58.81	89.23	15.11	47.11	83.56	97.57	80.19	97.02	77.95	96.92	75.06	94.49

TABLE XI: Clean accuracy of models in Tabs. II, VII and XIII. We report the results of a fixed random seed here.

	CIFAR10			ImageNette		
	Clean Acc		Generalization	Clean Acc		Generalization
	Train/Test	Gap (\downarrow)	Train/Test	Gap (\downarrow)	Train/Test	Gap (\downarrow)
<i>ST</i>	100.00/94.40	5.60	97.75/96.74	1.01		
<i>MU</i> , $\tau = 1$	100.00/95.04	4.96	95.53/97.10	-1.57		
<i>MU</i> , $\tau = 5$	100.00/96.13	3.87	84.23/97.58	-13.35		
<i>CM</i> , $\tau = 1$	100.00/95.45	4.55	94.84/97.10	-2.26		
<i>CM</i> , $\tau = 5$	99.99/95.93	4.06	82.46/97.73	-15.27		
<i>CO</i> , $\tau = 1$	100.00/95.09	4.91	97.40/96.94	0.46		
<i>CO</i> , $\tau = 5$	100.00/95.79	4.21	95.41/96.97	-1.56		
<i>LS</i> , $\tau = 1$	100.00/94.84	5.16	98.09/97.48	0.61		
<i>LS</i> , $\tau = 5$	100.00/94.35	5.65	98.38/98.04	0.34		
<i>AT</i>	100.00/94.30	5.70	96.15/95.99	0.16		
<i>IR</i>	100.00/92.76	7.24	97.24/96.13	1.11		
<i>JR</i>	100.00/94.46	5.54	97.51/96.28	1.23		
<i>ER</i>	100.00/92.83	7.17	97.86/97.12	0.74		
<i>SAM</i>	100.00/95.20	4.80	96.54/97.53	-0.99		
<i>SAM&IR</i>	99.87/92.72	7.15	95.49/96.51	-1.02		
<i>SAM&JR</i>	100.00/95.16	4.84	95.62/96.79	-1.17		

and y are unit vectors, i.e., $\|x\|_2 = \|y\|_2 = 1$. Let $\cos\langle x, y \rangle = \frac{x \cdot y}{\|x\|_2 \cdot \|y\|_2}$. Let c denote any real number. Then

$$\delta \cdot y < c - \epsilon \sqrt{2 - 2 \cos\langle x, y \rangle} \Rightarrow \delta \cdot x < c. \quad (3)$$

Proof. $\delta \cdot x = \delta \cdot y + \delta \cdot (x - y) < c - \epsilon \sqrt{2 - 2 \cos\langle x, y \rangle} + \delta \cdot (x - y)$. By law of cosines, $\delta \cdot (x - y) \leq \|\delta\|_2 \cdot \|(x - y)\|_2 \leq \epsilon \sqrt{2 - 2 \cos\langle x, y \rangle}$. Hence, $\delta \cdot x < c$ \square

Lemma 2. For arbitrary events A and B , we have $\Pr(\neg A \cap \neg B) \geq 1 - \Pr(A) - \Pr(B)$, where $\Pr(\cdot)$ denotes the probability of a event.

Proof. For events A and B , we have $\Pr(A \cup B) + \Pr(\neg(A \cup B)) = 1$. And it’s true that $\Pr(A) + \Pr(B) \geq \Pr(A \cup B)$ and $\neg(A \cup B) = \neg A \cap \neg B$. Then we have $\Pr(A) + \Pr(B) + \Pr(\neg A \cap \neg B) \geq \Pr(A \cup B) + \Pr(\neg(A \cup B)) = 1$, thus $\Pr(\neg A \cap \neg B) \geq 1 - \Pr(A) - \Pr(B)$. \square

Note that this is a generalizable property. Given any number of events A_1, A_2, \dots, A_n , we can also have $\Pr(A_1) + \Pr(A_2) + \dots + \Pr(A_n) + \Pr(\neg A_1 \cap \neg A_2 \dots \cap \neg A_n) \geq 1$, thus $\Pr(\neg A_1 \cap \neg A_2 \dots \cap \neg A_n) \geq 1 - \Pr(A_1) - \Pr(A_2) - \dots - \Pr(A_n)$.

Proof for Theorem 1

The proof builds upon the derivations in Yang *et al.* [65], with the primary modifications focusing on the definition of smoothness. We omit some intermediate steps to save space.

Proof. Define auxiliary function $f, g : \mathcal{M} \times \mathcal{L} \rightarrow \mathbb{R}$ such that

$$f(x, y) = \frac{\min_{y' \in \mathcal{L}: y' \neq y} \ell_{\mathcal{F}}(x + \delta, y') - \ell_{\mathcal{F}}(x, y) - \bar{\sigma}_{\mathcal{F}} \epsilon^2 / 2}{\|\nabla_x \ell_{\mathcal{F}}(x, y)\|_2},$$

$$g(x, y) = \frac{\min_{y' \in \mathcal{L}: y' \neq y} \ell_{\mathcal{G}}(x + \delta, y') - \ell_{\mathcal{G}}(x, y) + \bar{\sigma}_{\mathcal{G}} \epsilon^2 / 2}{\|\nabla_x \ell_{\mathcal{G}}(x, y)\|_2}. \quad (4)$$

The f and g are orthogonal to the confidence score functions of model \mathcal{F} and \mathcal{G} , we reuse the notation f here in the Appendix. Note that $c_{\mathcal{F}} = \min_{(x, y) \sim \mathcal{D}} f(x, y)$, $c_{\mathcal{G}} = \max_{(x, y) \sim \mathcal{D}} g(x, y)$.

Observing Definition 3, the transferability concern a successful transfer requiring 4 events, i.e., $\mathcal{F}(x) = y$, $\mathcal{G}(x) = y$, $\mathcal{F}(x + \delta) \neq y$, and $\mathcal{G}(x + \delta) \neq y$. In other words, both \mathcal{F} and \mathcal{G} give the correct prediction for x , and the wrong prediction for $x + \delta$, we have:

$$\begin{aligned} & \Pr(T_r(\mathcal{F}, \mathcal{G}, x, y) = 1) \\ &= \Pr(\mathcal{F}(x) = y \cap \mathcal{G}(x) = y \cap \mathcal{F}(x + \delta) \neq y \cap \mathcal{G}(x + \delta) \neq y) \\ &\geq 1 - \Pr(\mathcal{F}(x) \neq y) - \Pr(\mathcal{G}(x) \neq y) - \Pr(\mathcal{F}(x + \delta) = y) \\ &\quad - \Pr(\mathcal{G}(x + \delta) = y) \\ &\geq 1 - \gamma_{\mathcal{F}} - \gamma_{\mathcal{G}} - \alpha - \Pr(\mathcal{G}(x + \delta) = y). \end{aligned} \quad (5)$$

Here we use the general version for 4 events of Lemma 2 to derive the first inequality. Note that $\mathcal{F}(x) \neq y$, $\mathcal{G}(x) \neq y$, $\mathcal{F}(x + \delta) = y$ and $\mathcal{G}(x + \delta) = y$ are the corresponding complementary events of $\mathcal{F}(x) = y$, $\mathcal{G}(x) = y$, $\mathcal{F}(x + \delta) \neq y$, and $\mathcal{G}(x + \delta) \neq y$. In the second inequality, we use the definitions of the model risks $\gamma_{\mathcal{F}}$, $\gamma_{\mathcal{G}}$ and α ($\Pr(\mathcal{F}(x + \delta) = y) < \alpha$ holds, see Theorem 1). Now consider $\Pr(\mathcal{F}(x + \delta) = y)$

and $\Pr(\mathcal{G}(x + \delta) = y)$. Given that model predicts the label for which training loss is minimized, $\mathcal{F}(x + \delta) = y \iff \ell_{\mathcal{F}}(x + \delta, y) < \min_{y' \in \mathcal{L}: y' \neq y} \ell_{\mathcal{F}}(x + \delta, y')$. Similarly, $\mathcal{G}(x + \delta) = y \iff \ell_{\mathcal{G}}(x + \delta, y) < \min_{y' \in \mathcal{L}: y' \neq y} \ell_{\mathcal{G}}(x + \delta, y')$. Following Taylor’s Theorem with Lagrange remainder, we have

$$\ell_{\mathcal{F}}(x + \delta, y) = \ell_{\mathcal{F}}(x, y) + \delta \nabla_x \ell_{\mathcal{F}}(x, y) + \frac{1}{2} \xi^{\top} \mathbf{H}_{\mathcal{F}} \xi, \quad (6)$$

$$\ell_{\mathcal{G}}(x + \delta, y) = \ell_{\mathcal{G}}(x, y) + \delta \nabla_x \ell_{\mathcal{G}}(x, y) + \frac{1}{2} \xi^{\top} \mathbf{H}_{\mathcal{G}} \xi. \quad (7)$$

In Eq. (6) and Eq. (7), $\|\xi\| < \|\delta\|$. $\mathbf{H}_{\mathcal{F}}$ and $\mathbf{H}_{\mathcal{G}}$ are Hessian matrices of $\ell_{\mathcal{F}}$ and $\ell_{\mathcal{G}}$ respectively. Since $\ell_{\mathcal{F}}(x + \delta, y)$ and $\ell_{\mathcal{G}}(x + \delta, y)$ have upper smoothness $\bar{\sigma}_{\mathcal{F}}$ and $\bar{\sigma}_{\mathcal{G}}$, the maximum eigenvalues of $\mathbf{H}_{\mathcal{F}}$ and $\mathbf{H}_{\mathcal{G}}$ (both defined generally) are bounded. As the result, $|\xi^{\top} \mathbf{H}_{\mathcal{F}} \xi| \leq \bar{\sigma}_{\mathcal{F}} \cdot \|\xi\|_2^2 \leq \bar{\sigma}_{\mathcal{F}} \epsilon^2$. Applying them to Eq. (6) and Eq. (7), we thus have

$$\ell_{\mathcal{F}} + \delta \nabla_x \ell_{\mathcal{F}} - \frac{1}{2} \bar{\sigma}_{\mathcal{F}} \epsilon^2 \leq \ell_{\mathcal{F}}(x + \delta, y) \leq \ell_{\mathcal{F}} + \delta \nabla_x \ell_{\mathcal{F}} + \frac{1}{2} \bar{\sigma}_{\mathcal{F}} \epsilon^2, \quad (8)$$

$$\ell_{\mathcal{G}} + \delta \nabla_x \ell_{\mathcal{G}} - \frac{1}{2} \bar{\sigma}_{\mathcal{G}} \epsilon^2 \leq \ell_{\mathcal{G}}(x + \delta, y) \leq \ell_{\mathcal{G}} + \delta \nabla_x \ell_{\mathcal{G}} + \frac{1}{2} \bar{\sigma}_{\mathcal{G}} \epsilon^2. \quad (9)$$

Here we abbreviate the notations $\nabla_x \ell_{\mathcal{G}}(x, y)$ and $\nabla_x \ell_{\mathcal{F}}(x, y)$ as $\nabla_x \ell_{\mathcal{G}}$ and $\nabla_x \ell_{\mathcal{F}}$ respectively to save space, as often needed hereinafter. Apply right hand side of Eq. (8) to

$\Pr(\mathcal{F}(x + \delta) = y) \leq \alpha$:

$$\begin{aligned}
& \Pr(\mathcal{F}(x + \delta) = y) \\
&= \Pr\left(\ell_{\mathcal{F}}(x + \delta, y) < \min_{y' \in \mathcal{L}: y' \neq y} \ell_{\mathcal{F}}(x + \delta, y')\right) \\
&\geq \Pr\left(\ell_{\mathcal{F}} + \delta \nabla_x \ell_{\mathcal{F}} + \frac{1}{2} \bar{\sigma}_{\mathcal{F}} \epsilon^2 < \min_{y' \in \mathcal{L}: y' \neq y} \ell_{\mathcal{F}}(x + \delta, y')\right) \\
&= \Pr\left(\delta \cdot \frac{\nabla_x \ell_{\mathcal{F}}}{\|\nabla_x \ell_{\mathcal{F}}\|_2} < f(x, y)\right), \\
&\implies \Pr\left(\delta \cdot \frac{\nabla_x \ell_{\mathcal{F}}}{\|\nabla_x \ell_{\mathcal{F}}\|_2} < f(x, y)\right) \leq \alpha. \tag{10}
\end{aligned}$$

Apply left hand side of Eq. (9) to $\Pr(\mathcal{G}(x + \delta) = y)$:

$$\begin{aligned}
& \Pr(\mathcal{G}(x + \delta) = y) \\
&= \Pr\left(\ell_{\mathcal{G}}(x + \delta, y) < \min_{y' \in \mathcal{L}: y' \neq y} \ell_{\mathcal{G}}(x + \delta, y)\right) \\
&\leq \Pr\left(\ell_{\mathcal{G}} + \delta \nabla_x \ell_{\mathcal{G}} - \frac{1}{2} \bar{\sigma}_{\mathcal{G}} \epsilon^2 < \min_{y' \in \mathcal{L}: y' \neq y} \ell_{\mathcal{G}}(x + \delta, y)\right) \\
&= \Pr\left(\delta \cdot \frac{\nabla_x \ell_{\mathcal{G}}}{\|\nabla_x \ell_{\mathcal{G}}\|_2} < g(x, y)\right) \\
&\leq \Pr\left(\delta \cdot \frac{\nabla_x \ell_{\mathcal{G}}}{\|\nabla_x \ell_{\mathcal{G}}\|_2} < c_{\mathcal{G}}\right) \tag{11}
\end{aligned}$$

Eq. (11) use the definition of g in Eq. (4) and the definition of $c_{\mathcal{G}}$. Since $\|\delta\|_2 \leq \epsilon$, from Lemma 1 in Lemma 1, we can deduce

$$\delta \cdot \frac{\nabla_x \ell_{\mathcal{G}}}{\|\nabla_x \ell_{\mathcal{G}}\|_2} < f(x, y) - \epsilon \sqrt{2 - 2 \underline{\mathcal{S}}_{\mathcal{D}}(\ell_{\mathcal{F}}, \ell_{\mathcal{G}})} \tag{12}$$

$$\implies \delta \cdot \frac{\nabla_x \ell_{\mathcal{G}}}{\|\nabla_x \ell_{\mathcal{G}}\|_2} < f(x, y) - \epsilon \sqrt{2 - 2 \cos \langle \nabla_x \ell_{\mathcal{F}}, \nabla_x \ell_{\mathcal{G}} \rangle} \tag{13}$$

$$\implies \delta \cdot \frac{\nabla_x \ell_{\mathcal{F}}}{\|\nabla_x \ell_{\mathcal{F}}\|_2} < f(x, y). \tag{14}$$

From Eq. (12) to Eq. (13), the definition of $\underline{\mathcal{S}}_{\mathcal{D}}$ is used, since it indicates that $\underline{\mathcal{S}}_{\mathcal{D}}(\ell_{\mathcal{F}}, \ell_{\mathcal{G}}) \leq \cos \langle \nabla_x \ell_{\mathcal{F}}(x, y), \nabla_x \ell_{\mathcal{G}}(x, y) \rangle$. Eq. (13) to Eq. (14) uses the Lemma directly. As a result, using Eq. (10), we have

$$\begin{aligned}
& \Pr\left(\delta \cdot \frac{\nabla_x \ell_{\mathcal{G}}(x, y)}{\|\nabla_x \ell_{\mathcal{G}}(x, y)\|_2} < f(x, y) - \epsilon \sqrt{2 - 2 \underline{\mathcal{S}}_{\mathcal{D}}(\ell_{\mathcal{F}}, \ell_{\mathcal{G}})}\right) \\
&\leq \Pr\left(\delta \cdot \frac{\nabla_x \ell_{\mathcal{F}}(x, y)}{\|\nabla_x \ell_{\mathcal{F}}(x, y)\|_2} < f(x, y)\right) \leq \alpha.
\end{aligned}$$

Since $c_{\mathcal{F}} \leq f(x, y)$, we also have

$$\Pr\left(\delta \cdot \frac{\nabla_x \ell_{\mathcal{G}}(x, y)}{\|\nabla_x \ell_{\mathcal{G}}(x, y)\|_2} < c_{\mathcal{F}} - \epsilon \sqrt{2 - 2 \underline{\mathcal{S}}_{\mathcal{D}}(\ell_{\mathcal{F}}, \ell_{\mathcal{G}})}\right) \leq \alpha.$$

Given the minimum of $\delta \cdot \frac{\nabla_x \ell_{\mathcal{G}}(x, y)}{\|\nabla_x \ell_{\mathcal{G}}(x, y)\|_2}$ is lower bounded by $-\max \|\delta\|_2 = -\epsilon$. Therefore, its expectation can be bounded:

$$\mathbb{E}\left[\delta \cdot \frac{\nabla_x \ell_{\mathcal{G}}}{\|\nabla_x \ell_{\mathcal{G}}\|_2}\right] \geq -\epsilon \alpha + (c_{\mathcal{F}} - \epsilon \sqrt{2 - 2 \underline{\mathcal{S}}_{\mathcal{D}}(\ell_{\mathcal{F}}, \ell_{\mathcal{G}})}) (1 - \alpha). \tag{15}$$

According to Markov's inequality, from Eq. (15), we can

deduce that

$$\begin{aligned}
& \Pr\left(\delta \cdot \frac{\nabla_x \ell_{\mathcal{G}}}{\|\nabla_x \ell_{\mathcal{G}}\|_2} < c_{\mathcal{G}}\right) \\
&\leq \frac{\epsilon(1 + \alpha) - (c_{\mathcal{F}} - \epsilon \sqrt{2 - 2 \underline{\mathcal{S}}_{\mathcal{D}}(\ell_{\mathcal{F}}, \ell_{\mathcal{G}})}) (1 - \alpha)}{\epsilon - c_{\mathcal{G}}} \tag{16}
\end{aligned}$$

Combining Eq. (11) and Eq. (16), we have

$$\begin{aligned}
& \Pr(\mathcal{G}(x + \delta) = y) \\
&\leq \frac{\epsilon(1 + \alpha) - (c_{\mathcal{F}} - \epsilon \sqrt{2 - 2 \underline{\mathcal{S}}_{\mathcal{D}}(\ell_{\mathcal{F}}, \ell_{\mathcal{G}})}) (1 - \alpha)}{\epsilon - c_{\mathcal{G}}} \tag{17}
\end{aligned}$$

Thus, we conclude our proof by plugging Eq. (17) into Eq. (5). \square

D. Proof of connection between IR and JR

Proposition 1. Let a neural network parameterized by θ , and f_{θ} represents its logit network. Given a sample (x, y) , if $\|\nabla_x f_{\theta}(x)\|_F \rightarrow 0$, $\|\nabla_x \ell(f_{\theta}(x), y)\| \rightarrow 0$, where ℓ denotes the cross-entropy loss function.

Proof. Define the logit output of f_{θ} given input feature x with respect to each class as z_1, z_2, \dots, z_k , including the according logit of target class z_y . Accordingly, $\nabla_x f_{\theta}(x) = (z_1, z_2, \dots, z_k)^T$. Thus, we have

$$\|\nabla_x f_{\theta}(x)\|_F = \sum_i^k \|\nabla_x z_i\| \tag{18}$$

The cross-entropy loss of (x, y) is computed as follows:

$$\ell(f_{\theta}(x), y) = -\log\left(\frac{e^{z_y}}{\sum_i^k e^{z_i}}\right) = -z_y + \log\left(\sum_i^k e^{z_i}\right).$$

As a result, the gradient w.r.t. x $\nabla_x \ell(f_{\theta}(x), y)$ is

$$\nabla_x \ell(f_{\theta}(x), y) = -\nabla_x z_y + \frac{\sum_i^k e^{z_i} \nabla_x z_i}{\sum_i^k e^{z_i}}$$

Thus,

$$\begin{aligned}
\|\nabla_x \ell(f_{\theta}(x), y)\| &= \left\| \frac{1}{\sum_i^k e^{z_i}} \cdot \sum_i^k e^{z_i} \nabla_x z_i - \nabla_x z_y \right\| \\
&\leq \frac{1}{\sum_i^k e^{z_i}} \cdot \left\| \sum_i^k e^{z_i} \nabla_x z_i \right\| + \|\nabla_x z_y\| \\
&\leq \frac{1}{\sum_i^k e^{z_i}} \cdot \sum_i^k e^{z_i} \|\nabla_x z_i\| + \|\nabla_x z_y\| \\
&< \sum_i^k \|\nabla_x z_i\| + \|\nabla_x z_y\| \tag{19}
\end{aligned}$$

Note that if $\sum_i^k \|\nabla_x z_i\| \rightarrow 0$, $\|\nabla_x z_y\| \rightarrow 0$. Observing Eqs. (18) and (19), we can conclude that if $\|\nabla_x f_{\theta}(x)\|_F \rightarrow 0$, $\|\nabla_x \ell(f_{\theta}(x), y)\| \rightarrow 0$. \square

TABLE XII: Transfer ASRs of AEs crafted against different surrogates on **CIFAR-10** and **ImageNette** using **AutoAttack**. We plot this table in the same way as Tab. II. In %.

CIFAR-10													
	4/255				8/255				16/255				
	ResNet50	VGG16	InceptionV3	DenseNet121	ResNet50	VGG16	InceptionV3	DenseNet121	ResNet50	VGG16	InceptionV3	DenseNet121	
<i>ST</i>	41.2 \pm 5.6	30.1 \pm 3.5	41.7 \pm 5.3	58.6 \pm 7.1	62.9 \pm 7.9	54.5 \pm 6.5	64.8 \pm 6.0	80.5 \pm 6.8	83.2 \pm 5.2	81.0 \pm 5.5	84.2 \pm 3.8	91.0 \pm 3.3	
<i>MU</i> , $\tau = 1$	27.9 \pm 5.1	20.9 \pm 2.5	29.0 \pm 4.8	40.2 \pm 7.0	48.5 \pm 6.9	40.6 \pm 3.7	51.4 \pm 5.9	65.3 \pm 7.5	73.1 \pm 6.4	71.3 \pm 4.5	76.5 \pm 4.7	85.2 \pm 5.1	
<i>MU</i> , $\tau = 3$	20.4 \pm 0.6	16.4 \pm 0.5	23.3 \pm 1.2	27.8 \pm 1.6	37.7 \pm 0.9	31.2 \pm 1.1	42.0 \pm 1.4	51.1 \pm 1.3	68.0 \pm 1.9	64.7 \pm 1.7	72.9 \pm 1.2	80.4 \pm 1.2	
<i>MU</i> , $\tau = 5$	18.8 \pm 0.3	15.7 \pm 0.3	20.8 \pm 1.0	24.5 \pm 0.8	33.8 \pm 1.7	28.6 \pm 0.9	37.5 \pm 1.0	44.9 \pm 1.6	64.1 \pm 1.5	60.5 \pm 1.9	68.3 \pm 0.4	76.4 \pm 1.5	
<i>CM</i> , $\tau = 1$	22.4 \pm 0.9	16.7 \pm 1.3	21.8 \pm 0.6	30.3 \pm 1.3	39.6 \pm 1.7	32.4 \pm 2.5	39.0 \pm 1.0	53.4 \pm 2.5	64.5 \pm 2.0	62.4 \pm 3.2	64.9 \pm 1.7	77.8 \pm 3.2	
<i>CM</i> , $\tau = 3$	14.3 \pm 1.2	11.5 \pm 0.4	14.2 \pm 1.1	17.2 \pm 2.0	20.2 \pm 1.8	25.1 \pm 2.6	32.1 \pm 4.4	48.9 \pm 4.1	47.1 \pm 2.7	49.8 \pm 3.0	60.6 \pm 4.6		
<i>CM</i> , $\tau = 5$	12.3 \pm 0.5	10.4 \pm 0.2	12.0 \pm 1.1	13.7 \pm 1.2	21.9 \pm 1.8	17.5 \pm 0.6	21.3 \pm 0.9	26.5 \pm 1.8	44.4 \pm 1.6	41.5 \pm 1.6	44.3 \pm 1.9	53.4 \pm 1.8	
<i>CO</i> , $\tau = 1$	40.7 \pm 7.0	31.1 \pm 7.0	39.8 \pm 5.9	55.9 \pm 8.1	62.4 \pm 6.9	55.3 \pm 8.1	63.1 \pm 6.2	78.2 \pm 5.9	82.5 \pm 5.6	79.9 \pm 6.3	82.8 \pm 5.3	89.9 \pm 3.7	
<i>CO</i> , $\tau = 3$	34.6 \pm 5.2	24.9 \pm 2.8	33.7 \pm 5.1	47.1 \pm 8.0	55.5 \pm 5.8	46.0 \pm 4.7	55.8 \pm 6.7	70.7 \pm 8.0	79.6 \pm 5.4	74.4 \pm 5.1	79.2 \pm 5.6	86.8 \pm 5.0	
<i>CO</i> , $\tau = 5$	30.8 \pm 2.5	22.3 \pm 2.0	31.0 \pm 3.3	42.1 \pm 6.7	49.5 \pm 5.0	41.3 \pm 4.8	51.3 \pm 5.8	63.9 \pm 7.8	73.2 \pm 5.6	69.3 \pm 6.3	74.5 \pm 6.4	81.7 \pm 7.0	
<i>LS</i> , $\tau = 1$	35.5 \pm 4.8	28.2 \pm 5.7	35.5 \pm 3.3	48.4 \pm 5.7	54.3 \pm 9.4	49.7 \pm 10.7	56.0 \pm 6.4	69.4 \pm 8.4	76.1 \pm 7.8	76.9 \pm 8.3	78.3 \pm 6.0	85.9 \pm 5.1	
<i>LS</i> , $\tau = 3$	34.2 \pm 7.5	27.3 \pm 4.6	33.9 \pm 5.6	44.1 \pm 2.8	55.0 \pm 13.6	50.0 \pm 10.0	55.9 \pm 11.0	68.2 \pm 5.9	76.8 \pm 12.1	76.6 \pm 10.0	78.3 \pm 9.3	85.5 \pm 5.3	
<i>LS</i> , $\tau = 5$	31.3 \pm 3.5	26.6 \pm 3.5	30.2 \pm 3.1	41.2 \pm 2.9	51.1 \pm 8.2	48.6 \pm 8.0	51.2 \pm 6.9	65.6 \pm 7.0	72.2 \pm 7.7	74.5 \pm 8.2	73.5 \pm 6.2	83.3 \pm 5.4	
<i>AT</i>	54.4 \pm 2.3	45.3 \pm 1.5	49.5 \pm 3.6	61.0 \pm 3.5	80.2 \pm 5.8	73.7 \pm 5.9	77.5 \pm 4.1	86.4 \pm 4.2	90.8 \pm 3.0	89.5 \pm 3.2	89.8 \pm 2.8	92.9 \pm 2.3	
<i>IR</i>	51.9 \pm 1.4	45.3 \pm 1.1	48.0 \pm 0.6	54.4 \pm 1.1	85.9 \pm 3.4	82.4 \pm 3.9	83.8 \pm 3.3	87.4 \pm 3.2	92.4 \pm 2.1	92.2 \pm 2.3	91.8 \pm 2.1	92.0 \pm 2.0	
<i>JR</i>	63.5 \pm 8.7	53.1 \pm 7.1	62.4 \pm 5.7	75.1 \pm 4.5	78.9 \pm 6.8	73.7 \pm 6.1	79.5 \pm 4.1	88.7 \pm 2.6	87.6 \pm 4.3	87.2 \pm 3.9	88.1 \pm 2.4	92.1 \pm 2.1	
<i>ER</i>	55.0 \pm 5.5	42.9 \pm 5.6	46.2 \pm 7.4	55.2 \pm 13.8	82.3 \pm 5.5	74.1 \pm 7.9	76.1 \pm 8.8	81.1 \pm 12.2	90.6 \pm 4.0	89.3 \pm 4.6	88.9 \pm 4.0	89.8 \pm 4.4	
<i>SAM</i>	66.1 \pm 8.6	53.4 \pm 5.8	66.0 \pm 8.8	81.1 \pm 6.9	88.4 \pm 4.7	83.4 \pm 4.5	88.7 \pm 4.8	94.1 \pm 2.4	94.3 \pm 3.0	94.2 \pm 2.9	94.8 \pm 2.4		
<i>SAM&JR</i>	52.9 \pm 6.6	47.0 \pm 1.0	48.2 \pm 1.2	54.1 \pm 1.7	88.3 \pm 2.3	85.5 \pm 2.7	85.7 \pm 2.4	88.7 \pm 2.0	92.8 \pm 2.0	92.9 \pm 2.0	92.2 \pm 2.0	92.4 \pm 1.9	
<i>SAM&JR</i>	69.8 \pm 3.0	57.2 \pm 2.9	69.2 \pm 2.5	82.7 \pm 2.1	90.4 \pm 3.9	86.2 \pm 4.7	90.3 \pm 3.5	94.6 \pm 1.8	94.8 \pm 1.9	94.6 \pm 2.1	94.6 \pm 1.7	94.9 \pm 1.6	

ImageNette													
	4/255				8/255				16/255				
	VGG16	DenseNet121	MobileNetV2	Xception	VGG16	DenseNet121	MobileNetV2	Xception	VGG16	DenseNet121	MobileNetV2	Xception	
<i>ST</i>	10.1 \pm 0.7	16.0 \pm 1.0	7.1 \pm 0.5	6.7 \pm 0.1	27.4 \pm 3.0	41.0 \pm 2.8	17.7 \pm 0.7	16.9 \pm 1.1	61.5 \pm 6.5	83.3 \pm 4.9	51.5 \pm 2.7	44.8 \pm 4.6	
<i>MU</i> , $\tau = 1$	7.9 \pm 1.5	11.1 \pm 1.1	5.9 \pm 0.5	6.1 \pm 0.5	20.3 \pm 1.5	23.0 \pm 2.2	13.5 \pm 1.3	11.1 \pm 0.3	43.8 \pm 0.8	60.5 \pm 4.5	39.1 \pm 2.3	29.5 \pm 1.9	
<i>MU</i> , $\tau = 3$	6.8 \pm 0.4	7.8 \pm 0.6	5.1 \pm 0.5	5.5 \pm 0.5	13.3 \pm 0.9	14.3 \pm 0.9	8.7 \pm 0.9	9.0 \pm 0.8	30.8 \pm 2.8	35.6 \pm 1.6	26.4 \pm 2.2	19.3 \pm 1.7	
<i>MU</i> , $\tau = 5$	5.9 \pm 0.5	7.0 \pm 0.2	4.2 \pm 0.4	5.3 \pm 0.3	10.4 \pm 1.0	11.6 \pm 0.6	8.2 \pm 0.6	7.5 \pm 0.5	24.9 \pm 0.9	27.3 \pm 1.1	20.7 \pm 1.3	17.2 \pm 0.8	
<i>CM</i> , $\tau = 1$	7.3 \pm 0.7	9.1 \pm 1.1	5.3 \pm 0.3	5.7 \pm 0.3	15.3 \pm 0.7	17.9 \pm 1.5	9.3 \pm 0.7	8.6 \pm 0.4	33.1 \pm 1.7	44.0 \pm 3.6	25.6 \pm 2.0	18.7 \pm 0.9	
<i>CM</i> , $\tau = 3$	5.8 \pm 0.4	6.4 \pm 0.6	4.2 \pm 0.6	5.3 \pm 0.3	9.3 \pm 0.9	11.4 \pm 1.2	7.1 \pm 1.1	6.9 \pm 0.5	20.2 \pm 0.8	24.7 \pm 2.3	17.2 \pm 0.6	12.7 \pm 1.7	
<i>CM</i> , $\tau = 5$	4.5 \pm 0.3	5.7 \pm 0.5	3.8 \pm 0.4	4.7 \pm 0.3	7.9 \pm 0.5	8.5 \pm 0.7	5.7 \pm 0.3	6.3 \pm 0.7	16.6 \pm 1.0	16.9 \pm 0.9	14.7 \pm 1.3	9.9 \pm 0.7	
<i>CO</i> , $\tau = 1$	10.9 \pm 1.1	15.3 \pm 0.7	6.9 \pm 0.7	7.2 \pm 0.0	26.7 \pm 2.5	41.3 \pm 3.5	17.9 \pm 0.7	16.3 \pm 1.1	60.2 \pm 4.6	83.9 \pm 4.1	50.6 \pm 3.4	43.1 \pm 3.1	
<i>CO</i> , $\tau = 3$	10.3 \pm 1.5	14.6 \pm 0.2	7.2 \pm 0.4	7.6 \pm 0.4	26.3 \pm 1.9	40.3 \pm 2.3	18.9 \pm 0.9	15.7 \pm 3.3	59.6 \pm 3.4	82.4 \pm 1.6	51.2 \pm 5.4	42.1 \pm 4.3	
<i>CO</i> , $\tau = 5$	9.7 \pm 1.3	13.2 \pm 0.4	6.2 \pm 0.0	4.6 \pm 0.4	24.4 \pm 3.2	35.4 \pm 4.6	14.8 \pm 0.8	15.0 \pm 0.4	58.2 \pm 5.4	79.9 \pm 2.1	39.8 \pm 1.6		
<i>LS</i> , $\tau = 1$	5.9 \pm 0.7	7.7 \pm 0.3	4.7 \pm 0.9	5.2 \pm 0.2	11.1 \pm 1.1	14.2 \pm 1.0	8.1 \pm 0.5	7.9 \pm 0.3	24.8 \pm 0.8	32.8 \pm 0.6	22.8 \pm 1.6	15.5 \pm 0.9	
<i>LS</i> , $\tau = 3$	4.9 \pm 0.3	6.4 \pm 0.2	4.1 \pm 0.7	5.2 \pm 0.4	9.5 \pm 0.3	11.7 \pm 0.7	7.3 \pm 0.3	7.1 \pm 0.3	22.0 \pm 0.6	26.6 \pm 1.0	19.4 \pm 0.8	14.3 \pm 1.9	
<i>LS</i> , $\tau = 5$	5.1 \pm 0.5	5.7 \pm 0.5	3.9 \pm 0.1	4.8 \pm 0.0	8.6 \pm 1.8	9.6 \pm 1.2	6.5 \pm 0.7	6.9 \pm 0.9	18.1 \pm 2.5	22.8 \pm 0.2	17.2 \pm 2.2	14.1 \pm 0.5	
<i>AT</i>	11.3 \pm 0.9	15.7 \pm 0.9	11.4 \pm 0.6	15.1 \pm 0.5	50.3 \pm 5.9	68.9 \pm 2.5	57.8 \pm 5.0	51.8 \pm 3.6	97.1 \pm 0.3	95.5 \pm 1.1	93.8 \pm 0.8		
<i>IR</i>	19.1 \pm 6.1	29.9 \pm 6.3	16.7 \pm 5.1	16.7 \pm 4.7	60.7 \pm 14.7	82.7 \pm 9.5	64.1 \pm 16.7	55.9 \pm 13.5	91.2 \pm 7.6	96.2 \pm 0.8	92.0 \pm 5.6	90.3 \pm 6.5	
<i>JR</i>	23.4 \pm 2.2	37.3 \pm 2.3	20.0 \pm 1.8	19.1 \pm 1.1	67.3 \pm 3.5	88.2 \pm 0.5	66.6 \pm 1.8	57.7 \pm 3.5	93.1 \pm 1.5	97.4 \pm 0.4	93.5 \pm 0.3	91.9 \pm 1.1	
<i>ER</i>	12.1 \pm 2.7	19.6 \pm 2.4	7.5 \pm 0.5	8.1 \pm 1.5	32.5 \pm 9.3	51.9 \pm 9.5	22.1 \pm 4.5	21.5 \pm 5.5	65.7 \pm 17.9	89.2 \pm 5.2	55.0 \pm 8.4	50.1 \pm 11.9	
<i>SAM</i>	22.6 \pm 2.6	30.1 \pm 0.5	12.7 \pm 0.5	11.5 \pm 0.1	55.5 \pm 1.9	72.5 \pm 3.1	39.4 \pm 3.4	34.8 \pm 3.0	89.8 \pm 1.0	97.1 \pm 0.7	86.1 \pm 10.3	82.0 \pm 13.8	
<i>SAM&JR</i>	23.7 \pm 4.1	37.5 \pm 2.3	22.0 \pm 2.8	19.7 \pm 1.5	68.9 \pm 8.3	91.1 \pm 2.3	73.5 \pm 6.9	64.3 \pm 7.5	94.6 \pm 1.3	96.9 \pm 0.5	95.4 \pm 1.2	94.1 \pm 1.3	</

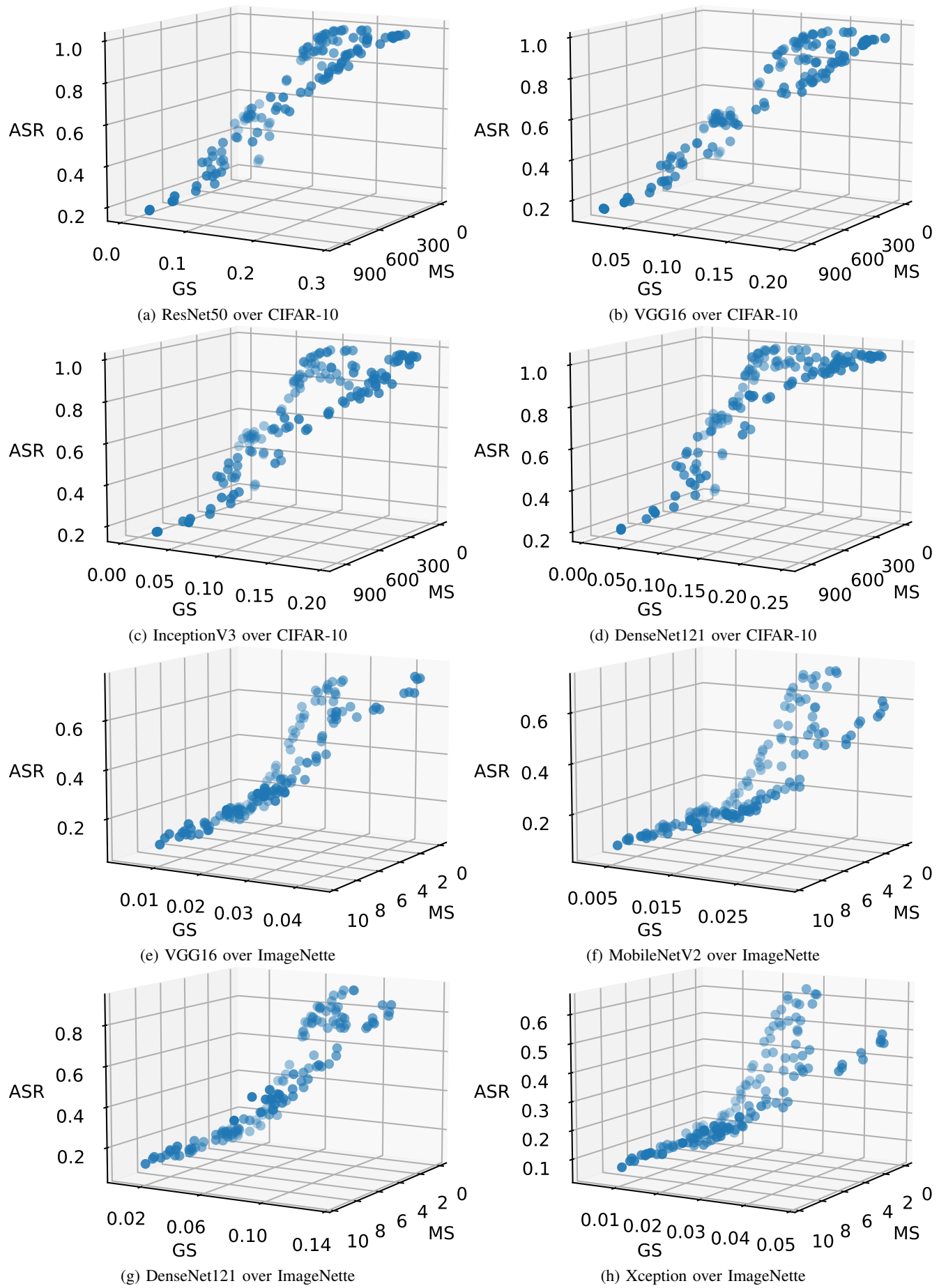


Figure 12: Correlation between (MS, GS) and ASR